The soil-borne white root rot pathogen *Rosellinia necatrix* expresses antimicrobial proteins during host colonization

Edgar A. Chavarro-Carrero[1,2], Nick C. Snelders[2,3,$], David E. Torres[1,3,$], Anton Kraege[2], Ana López-Moral[2], Gabriella C. Petti[2], Wilko Punt[2], Jan Wieneke[2], Rómulo García-Velasco[4], Carlos J. López-Herrera[5], Michael F. Seidl[3,#] and Bart P.H.J. Thomma[1,2,#,‡]

[1]Laboratory of Phytopathology, Wageningen University & Research, 6708 PB Wageningen, The Netherlands.

[2]Institute for Plant Sciences, Cluster of Excellence on Plant Sciences (CEPLAS), University of Cologne, Cologne, Germany

[3]Theoretical Biology & Bioinformatics Group, Department of Biology, Utrecht University, Utrecht, The Netherlands

[4]Laboratory of Phytopathology, Tenancingo University Center, Autonomous University of the State of Mexico, Tenancingo, State of Mexico, Mexico.

[5]CSIC, Instituto de Agricultura Sostenible, Dept. Protección de Cultivos, C/Alameda del Obispo s/n, 14004, Córdoba, Spain.

Short title: *Rosellinia necatrix* antimicrobial effector proteins

[$]These authors contributed equally

[#]These authors contributed equally

[‡]Corresponding author: B.P.H.J. Thomma; Telephone: 0049-221-47089261; E-mail: bthomma@uni-koeln.de

ABSTRACT

Rosellinia necatrix is a prevalent soil-borne plant-pathogenic fungus that is the causal agent of white root rot disease in a broad range of host plants. The limited availability of genomic resources for *R. necatrix* has complicated a thorough understanding of its infection biology. Here, we sequenced nine *R. necatrix* strains with Oxford Nanopore sequencing technology, and with DNA proximity ligation we generated a gapless assembly of one of the genomes into ten chromosomes. Whereas many filamentous pathogens display a so-called two-speed genome with more dynamic and more conserved compartments, the *R. necatrix* genome does not display such genome compartmentalization. It has recently been proposed that fungal plant pathogens may employ effectors with antimicrobial activity to manipulate the host microbiota to promote infection. In the predicted secretome of *R. necatrix*, 26 putative antimicrobial effector proteins were identified, nine of which are expressed during plant colonization. Two of the candidates were tested, both of which were found to possess selective antimicrobial activity. Intriguingly, some of the inhibited bacteria are antagonists of *R. necatrix* growth *in vitro* and can alleviate *R. necatrix* infection on cotton plants. Collectively, our data show that *R. necatrix* encodes antimicrobials that are expressed during host colonization and that may contribute to modulation of host-associated microbiota to stimulate disease development.

46 **INTRODUCTION**

47 *Rosellinia necatrix* is a prevalent soil-borne plant-pathogenic fungus that is found
48 in temperate and tropical areas worldwide (Sivanesan and Holliday, 1972). As
49 causal agent of white root rot disease, *R. necatrix* has a broad host range
50 comprising at least 170 species of dicotyledonous angiosperms that are
51 dispersed over 63 genera and 30 families (Sztejnberg and Madar, 1980). Many of
52 these species are of great economic importance, such as *Coffea* spp. (coffee),
53 *Malus* spp. (apple), *Olea europea* L. (olive), *Persea americana* Mill. (avocado),
54 *Prunus* spp. (peaches, almonds, etc.), *Vitis vinifera* L. (grape) (Eguchi et al.,
55 2009) and *Rosa* sp. (rose) (García-Velasco et al., 2012).

56 Plants infected by *R. necatrix* usually display two types of symptoms. The
57 first type is displayed below-ground on the root system, where white and black
58 colonies of mycelium can occur on the surface of infected roots. As the fungus
59 penetrates and colonizes the root tissue, the roots acquire a dark brown color
60 (Guillaumin et al., 1982). The second type of symptom occurs above-ground.
61 These symptoms can develop rapidly because of the damaged root system and
62 comprise wilting of leaves, typically after a period of drought or physiological
63 stress, which affects plant vigor and eventually can lead to plant death.
64 Symptoms of *R. necatrix* infection can also appear slowly, leading to a decline in
65 growth, decreasing leaf numbers, along with wilting of leaves, chlorosis, and
66 death of twigs and branches. On perennials these symptoms aggravate over
67 time, and when moisture and temperature are unfavorable, the plant eventually
68 dies (Guillaumin et al., 1982).

69 Various studies have addressed the biology of *R. necatrix* (Pérez-Jiménez
70 et al., 2002; Pliego et al., 2009). Nevertheless, the molecular mechanisms
71 underlying pathogenicity of *R. necatrix* remain largely unexplored, mainly

because the limited availability of genomic resources to date complicates investigations into the molecular biology of *R. necatrix* infections. Until recently, only a single Illumina technology short-read sequencing-based *R. necatrix* draft genome assembly was generated of strain W97 that was isolated from apple in Japan (Shimizu et al., 2018). This 44 Mb genome assembly is highly fragmented as it comprises 1,209 contigs with 12,444 predicted protein-coding genes (Shimizu et al., 2018). Recently, another assembly was released of a South-African strain (CMW50482) that was isolated from avocado, yet this assembly is even more fragmented with 1,362 contigs (Wingfield et al., 2022).

It is generally accepted that plant pathogens secrete dozens to hundreds of so-called effectors into their host plants to stimulate host colonization (Rovenich et al., 2014; Wilson and McDowell, 2022). Effectors can be defined as small, secreted proteins of ≤300 amino acids that are cysteine-rich and have tertiary structures that are stabilized by disulfide bridges and that are secreted by pathogens to promote disease on plant hosts (Duplessis et al., 2011; Gan et al., 2013; Stergiopoulos et al., 2013; Lo Presti et al., 2015). However, also larger secreted proteins have been found to act as effectors, such as several LysM effectors (Djamei et al., 2011; Kombrink and Thomma, 2013). Furthermore, also non-proteinaceous effectors have been described, such as fungal secondary metabolites as well as small RNA (sRNA) molecules that are delivered into host cells to suppress host immunity (Weiberg et al., 2014). Many effectors have been shown to act in suppression of host immune responses (Rovenich et al., 2014). However, recent studies have uncovered additional functions of pathogen effector proteins in host colonization (Wilson and McDowell, 2022). For example, the soil-borne pathogen *Verticillium dahliae* secretes effector proteins to modulate microbiota compositions inside the host

98 plant as well as outside the host in the soil to support host colonization (Snelders
99 et al., 2020; 2021; 2022; 2023). One of them is the effector protein VdAve1 that
100 was shown to display selective antimicrobial activity and facilitate colonization of
101 tomato and cotton plants through host microbiota manipulation by suppressing
102 antagonistic bacteria, such as members of the *Spingomonadaceae* (Snelders et
103 al., 2020). Besides VdAve1, ten additional potentially antimicrobial effector
104 protein candidates were predicted by mining the *V. dahliae* secretome for
105 structural homologues of known antimicrobial proteins (AMPs) (Snelders et al.,
106 2020). One of these candidates, VdAMP2, was subsequently found to contribute
107 to *V. dahliae* survival in soil through its efficacy in microbial competition
108 (Snelders et al., 2020). Another candidate, VdAMP3, was shown to promote
109 microsclerotia formation in decaying host tissue through its antifungal activity
110 directed against fungal niche competitors (Snelders et al., 2021). Most recently,
111 a multiallelic gene homologous to *VdAve1* was identified as *VdAve1-like*
112 (*VdAve1L*) of which the *VdAve1L2* variant was shown to encode an effector that
113 promotes tomato colonization through suppression of antagonistic Actinobacteria
114 in the host microbiota (Snelders et al., 2023). These findings have led to the
115 hypothesis that microbiota manipulation is a general virulence strategy of plant
116 pathogens to promote host colonization (Snelders et al., 2022). However, thus
117 far evidence for such activity has been lacking for other fungal plant pathogens.

118 Similar to *V. dahliae*, also *R. necatrix* is a soil-borne pathogen that spends
119 at least part of its life cycle in the soil, known to be an extremely competitive
120 and microbe-rich environment (Smercina et al., 2021). In the present study, we
121 aimed to generate a high-quality genome assembly to mine the *R. necatrix*
122 genome for potential antimicrobial proteins that are exploited during host
123 colonization and test the hypothesis that other pathogenic fungi besides *V.*

124 *dahliae* exploit effector proteins with antimicrobial activity during host
125 colonization as well.

126 **RESULTS**

127 **A chromosome-level assembly of *Rosellinia necatrix* strain R18**

128 Thus far, two fragmented *R. necatrix* draft genome assemblies that comprise
129 over 1,200 contigs are publicly available (Shimizu et al., 2018; Wingfield et al.,
130 2022). To generate additional and more contiguous *R. necatrix* genome
131 assemblies, we sequenced nine strains of *R. necatrix* that were collected from
132 rose and avocado in Mexico and Spain, respectively, with Oxford Nanopore
133 sequencing technology (ONT). This resulted in genome assemblies of 28 (for
134 strain R18) to 399 (for strain CH12) contigs (Table 1). The most contiguous
135 assembly was obtained for strain R18, isolated from infected rose plants in
136 Mexico.

137

138 **Table 1. Sequencing summary and genome assembly statistics for nine**
139 ***Rosellinia necatrix* strains.**

Strain name	Rn19[a]	CH12[a]	Rn400[a]	R10[a]	R25[a]	R27[a]	R28[a]	R30[a]	R18[a]	R18[b]
Isolated from	Avocado	Avocado	Avocado	Rose	Rose	Rose	Rose	Rose	Rose	
Country of origin	Spain	Spain	Spain	Mexico	Mexico	Mexico	Mexico	Mexico	Mexico	
Read N50 (kb)	23	17	21	18	16	21	21	9	18	**30**
Coverage	45X	46X	35X	35X	45X	46X	41X	52X	42X	**120X**
No. of contigs	35	399	37	50	58	31	47	130	28	**11**
Total length (Mb)	48.2	49.9	48.2	48.9	49.2	49.2	48.7	48.3	49	**49.1**
Average length (Mb)	1.3	0.1	1.3	1	0.8	1.5	1	0.3	0.8	**4**
Maximum length (Mb)	6.4	6.3	5.8	4.4	4	6.4	6.4	4.5	4	**7.1**
N50 (Mb)	3.4	4.6	3.8	1.9	2.5	3.2	3.4	1.6	3.1	**5.1**
N90 (Mb)	0.8	3.1	1.3	0.4	0.5	1.2	0.8	0.3	0.6	**3.3**
GC (%)	46.28	46.37	46.37	45.35	45.49	45.43	45.50	45.99	45.35	**45.46**

140 [a]*de novo* assembly based on Nanopore sequencing of HMW DNA.
141 [b]*de novo* assembly based on Nanopore sequencing of HMW and UHMW DNA and Hi-C sequencing.

142

143 To further improve the genome assembly of strain R18, additional ONT
144 sequencing was performed using ultra HMW (UHMW) DNA as template.

145 Additionally, chromosome conformation capture (Hi-C) followed by high-
146 throughput sequencing was performed (Burton et al., 2013; Varoquaux et al.,
147 2015). Based on these orthogonal sequencing data, we ultimately assembled the
148 R18 genome into 11 contigs (Table 1). Using Tapestry (Davey et al., 2020)
149 twenty telomeric regions ([TTAGGG]*n*) were identified (Fig. 1A), and ten of the
150 11 contigs were found to contain telomeric regions at both ends, suggesting that
151 these represent completely assembled chromosomes, which could be confirmed
152 by Hi-C analysis (Fig. 1B). The 11th, and smallest, contig contained no telomeric
153 regions, displayed a markedly higher coverage (read depth) (Fig. 1B), and BLAST
154 analysis revealed hits to fungal mitochondrial genomes, showing that this contig
155 belongs to the mitochondrial genome. Accordingly, no mitochondrial genes could
156 be found on any of the ten chromosomal contigs. Thus, we conclude that our
157 assembly contains ten complete chromosomes that compose the nuclear
158 genome, and an 11th contig that composes the mitochondrial genome, and thus
159 that we generated a gapless, telomere-to-telomere, genome assembly. To
160 measure the completeness of the genome assembly, we used BUSCO v4 with the
161 Ascomycota dataset (Simão et al., 2015), which resulted in a completeness score
162 of 97%.

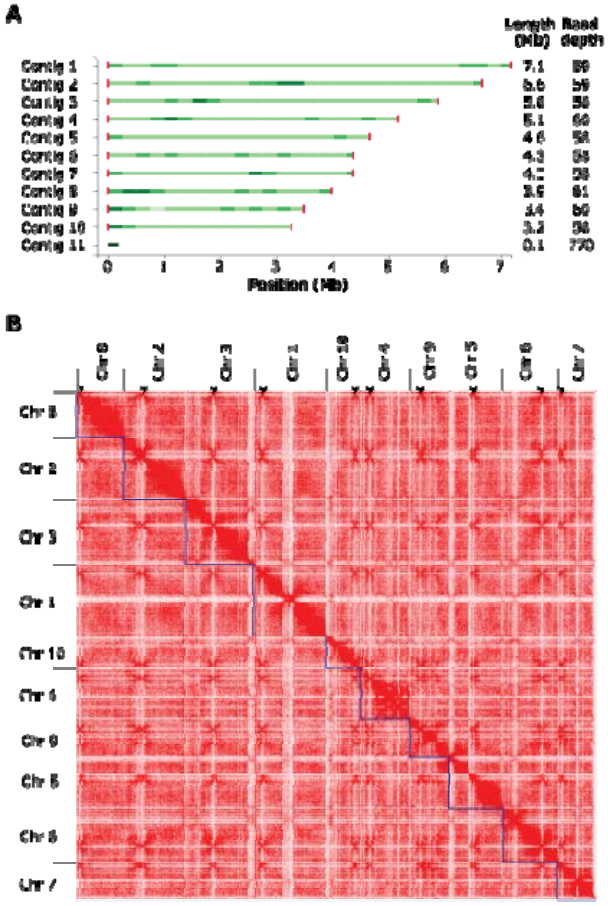

Figure 1. Genome assembly of *Rosellinia necatrix* strain R18. (A) Genome assembly plot generated with Tapestry (Davey et al., 2020). Green bars indicate contig sizes with the color intensity correlating with read coverage, while red bars indicate telomeres with the color intensity correlating with the number of telomeric repeats. Contig 11 lacks telomeres and represents the mitochondrial genome. (B) Hi-C contact matrix showing interaction frequencies between regions in the genome of *Rosellinia necatrix* strain R18. Ten regions with high inter-chromosomal interaction frequencies are indicative of centromeres and are indicated with arrowheads.

To further explore the *R. necatrix* strain R18 assembly, genome annotation was performed using Funannotate (Palmer and Stajich, 2017) guided by publicly available RNAseq data (Shimizu et al., 2018), resulting in 11,760 predicted protein-coding genes (Table 2). Furthermore, effector genes were predicted using EffectorP (Sperschneider et al., 2018). The assembled genome of *R. necatrix* strain R18 was predicted to encode 1,126 secreted proteins, of which 192 were predicted to be effector candidates. BLAST searches revealed that 182

180 of these have homology to Ascomycete fungal proteins, of which 69 had
181 functional domain annotations, while the remaining 113 were annotated as
182 hypothetical proteins (Supplemental Table 1). The largest group of annotated
183 effectors were cell wall degrading enzymes, including glycoside hydrolases and
184 carbohydrate esterases that are generally involved in plant cell wall degradation
185 (Underwood, 2012; Malinovsky et al., 2014). Effectors carrying carbohydrate-
186 binding domains while lacking enzymatic domains, specifically a concanavalin A-
187 like lectin and two cell wall integrity and stress response component (WSC)
188 domain-containing proteins, were also found. Concanavalin A-like lectin has been
189 described as a virulence factor, although no molecular mechanism has been
190 presented (Ismail and Able, 2016), while WSC domain-containing proteins can
191 protect fungal cell wall through structural strengthening, but their contribution to
192 plant colonization remains unclear (Wawra et al., 2019). Additionally, two lysin
193 motif (LysM) effectors were found that typically bind chitin and play roles in
194 virulence through suppression of chitin-triggered immunity or shielding hyphae
195 against host-derived chitinases (de Jonge et al., 2010; Kombrink and Thomma,
196 2013; Tian et al., 2021; 2022). Four genes were found to encode hydrophobins;
197 proteins that have been implicated in virulence through acting as phytotoxin
198 (Takai, 1974), or promoting attachment to plant surfaces and appressoria
199 formation (Talbot et al., 1996), although negative impacts on host colonization
200 have also been reported (Luciano-Rosario et al., 2022). Finally, three potential
201 toxins were found, namely a cerato-platanin domain-containing protein (Carresi
202 et al., 2006) and two necrosis and ethylene-inducing-like (NLP) effectors that are
203 typically thought to be phytotoxic to eudicot plants (Lenarčič et al., 2017; Seidl &
204 van den Ackerveken, 2019) (Supplemental Table 1).
205

206 **Table 2. Genome annotation of *Rosellinia necatrix* strain R18.**

Genomic trait	Value
Protein-coding genes (Funannotate version 1.8.13, Palmer and Stajich, 2017)	11,760
Mean gene length (bp)	1,689.48
Mean exons per gene	2.92
Mean intergenic length (bp)	1,114
Homologs in InterPro database	8,125
Secreted proteins (SignalP; version 5.0, Almagro et al., 2019)	1,126
Effectors (EffectorP; version 2.0, Sperschneider et al., 2018)	192
CAZymes (Funannotate)	535
CAZymes (secreted) (Funannotate)	300
Small cysteine-rich proteins (Funannotate)	209
LysM (lysin motif) effectors (Funannotate)	2
NLP (necrosis and ethylene-inducing-like) effectors (Funannotate)	2
Secondary metabolite clusters (antiSMASH; version 5.0, Blin et al., 2019)	48

207

208 Besides proteinaceous effectors, 48 secondary metabolite gene clusters
209 were predicted using the fungal version of antiSMASH (Blin et al., 2019; Table
210 2). From these, 13 showed homology to known secondary metabolite clusters,
211 including those for the production of swainsonine, cytochalasin E/K, pyriculol,
212 enniatin, and naphthalene, which have been implicated in pathogenicity through
213 their phytotoxic activity (Thomas, 1978; Sawai et al., 1983; Walton, 1990;
214 Shimizu et al., 2014; Cook et al., 2017; Zhao et al., 2019; Xu et al., 2021), and
215 copalyl diphosphate which has been implicated in elongation disorders in plants
216 (Rademacher and Graebe, 1979; Kawaide, 2006) (Supplemental Table 2).

217

218 **Absence of distinctive genome compartmentalization**

219 In many filamentous pathogens, effector genes are found in repeat-rich and gene
220 sparse genomic compartments, whereas they are depleted in repeat-poor and
221 gene-dense regions that typically harbor housekeeping genes, a genome
222 organization that is typically referred to as the two-speed genome (Frantzeskakis

223 et al., 2020). Thus, we aimed to explore if effector genes were associated with
224 repetitive regions in *R. necatrix* too. Interestingly, the repeat content in *R.*
225 *necatrix* strain R18 is low (2.39%) and evenly distributed throughout the
226 genome, with the most abundant families being DNA/Helitron (67%) and long
227 terminal repeats (LTRs; 31%). Accordingly, most repetitive elements are not
228 preferentially located near effectors ($p>0.05$ after permutation test for distance).
229 Moreover, effector genes are not preferentially found in regions with large
230 intergenic distances (Fig. 2). Thus, our results do not support association of
231 effector genes with repeat-rich regions in *R. necatrix*.

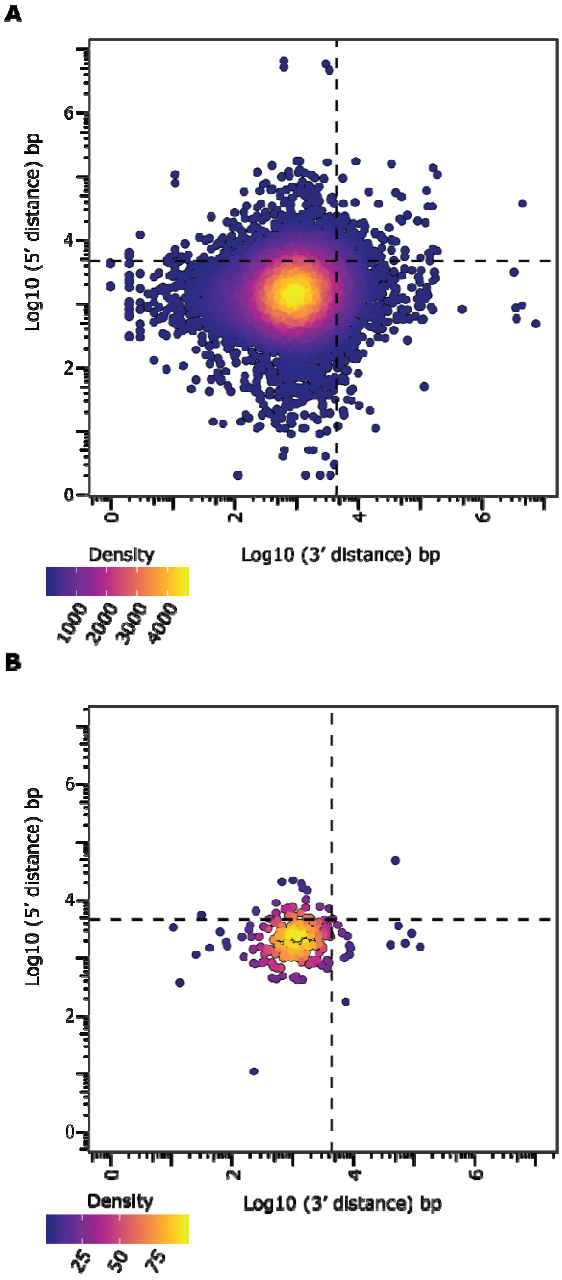

Figure 2. **Effector genes do not localize in gene-sparce regions.** Gene density plot of '5 and '3 flanking log10 transformed intergenic distance with the dashed lines depicting the mean intergenic distances for all genes (A) and candidate effector genes encoded in the *R. necatrix* genome (B).

Genomic comparisons in various filamentous fungi have revealed extensive chromosomal rearrangements and structural variants (SVs) in close association with effector genes (Torres et al., 2020; Faino et al., 2016; Oggenfuss et al.,

241 2021; Fouché et al., 2020; Shi-Kunne et al., 2018). Thus, we tested whether
242 effector genes are associated with SVs in *R. necatrix*. First, to explore the
243 genomic diversity among *R. necatrix* strains, a phylogenetic tree of all genomes
244 was constructed with Realphy (version 1.12) (Bertels *et al.,* 2014). Two clusters
245 were identified, one with strains from Mexico isolated from roses, and one cluster
246 with the strains from Spain and South Africa, isolated from avocado, as well as
247 Japan, isolated from apple (Fig. 3). This suggest that geographic origin of the
248 strains correlates with their phylogenetic relationship. Then, SVs were predicted
249 for each of the genomes sequenced in this study using NanoSV (version 1.2.4
250 with default settings; Stancu et al., 2017) by identifying split- and gapped-
251 aligned long reads for the various strains to define breakpoint-junctions of
252 structural variations when using the gapless genome assembly of strain R18 as a
253 reference. We retrieved 2,639 SVs in total, comprising 1,264 insertions, 1,344
254 deletions, 4 inversions and 27 translocations (Fig. 3A). The number of SVs per
255 strain corresponds to their phylogenetic relationships based on whole-genome
256 comparisons. To investigate the occurrence of the SVs in the *R. necatrix* strains,
257 we calculated the frequency of each SV over the strains used in the analysis.
258 Most of the SVs (94.2%) are shared by <50% of the strains, meaning that they
259 occur in less than four strains. This suggests that SV is a common phenomenon
260 in line with the phylogenetic and geographic relationship of *R. necatrix* strains.
261 Interestingly, SVs occur all across the genome (Fig. 3B), largely independently of
262 repetitive regions ($p>0.05$ after permutation test for distance), but are found in
263 close association with effector genes ($p<0.05$ after permutation test for
264 distance). Collectively, our results for *R. necatrix* substantiate the lack of the
265 typical genome compartmentalization that is associated with the two-speed

genome organization that was found in many other filamentous fungi (Raffaele and Kamoun, 2012).

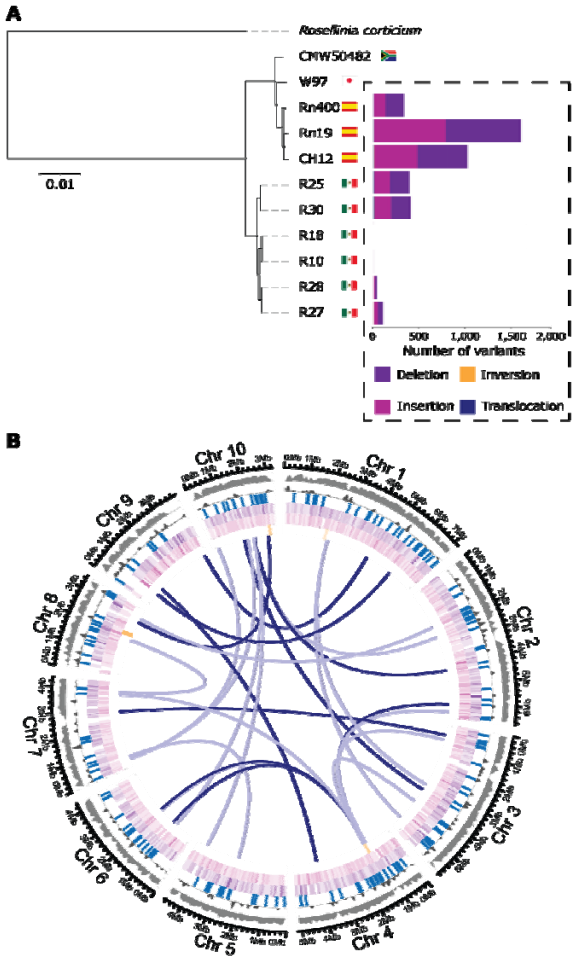

Figure 3. Phylogeny and structural variation of nine *Rosellinia necatrix* strains. (A) Phylogeny of sequenced *R. necatrix* strains was inferred using Realphy (Langmead and Salzberg, 2012), where branch lengths represent sequence divergence. *Rosellinia corticium* was used to root the tree. The amount of structural variants was calculated using NanoSV (Stancu et al., 2017) using strain R18 as a reference. (B) Circular plot displaying the genomic distribution of 2,019 SVs along the 10 chromosomes of *R. necatrix*. The tracks are shown in the following order from outside to inside: Gene density (10 kb), repetitive density (10 kb), effector gene locations, deletions, insertions and inversions and translocations. The color intensity of the lines for each SV track depict frequency in the *R. necatrix* collection.

Weak structural clustering in the effector catalog

281 Effectors continuously evolve towards optimal functionality while simultaneously
282 evading recognition by plant immune receptors, which is considered one of the
283 reasons for the lack of sequence conservation among effector proteins. Despite
284 this lack of sequence conservation, groups of effector proteins that share their
285 three-dimensional structure have been identified in various pathogenic fungi,
286 such as the MAX-effector (*Magnaporthe* Avrs and ToxB like) family of the rice
287 blast fungus *Magnaporthe oryzae* (de Guillen et al., 2015) that, together with
288 some other families, are also found in the scab fungus *Venturia inaequalis*
289 (Rocafort et al., 2022). It has been speculated that MAX effectors exhibit this
290 structural conservation as an adaptation either to the apoplastic environment, or
291 for transport into the plant cytosol (de Guillen et al., 2015). To investigate
292 whether subsets of *R. necatrix* effectors display a similar fold conservation, their
293 structures were predicted with Alphafold2 and clustered based on similarity (Fig.
294 4A). This analysis revealed that almost 40 percent of the effector candidates are
295 structurally unique, while the remaining effectors could be assigned to a total of
296 31 clusters. As these clusters were only small, with on average only four
297 members, we conclude that relatively little clustering occurs among *R. necatrix*
298 effectors.

299 To examine whether the observed clustering is merely based on structural
300 similarity, or is mainly driven by sequence conservation, the five largest clusters
301 that contain six to 11 members were further analysed (Fig. 4B, 4C). Two of the
302 five cluster show high average template modelling (TM) scores, with 0.85 and
303 0.91, respectively, on a scale from 0-1, while also showing a relatively high
304 degree of sequence conservation of 43 and 47 percent, respectively. The other
305 three clusters exhibit lower sequence conservation, with maximum 21 percent,
306 but also show considerably lower respectively structural conservation, with TM

307 scores between 0.57 and 0.64 only, indicating that structural similarity within the
308 clusters is positively correlating with sequence conservation. Hence, the
309 structural clustering can be explained by the sequence conservation amongst the
310 effector proteins. Taken together, although a considerable number of structural
311 effector clusters can be observed in *R. necatrix*, they contain only few members
312 and structural conservation is mostly based on sequence conservation. Thus,
313 effector family expansion seems to have played only a minor role in *R. necatrix*
314 effector evolution.

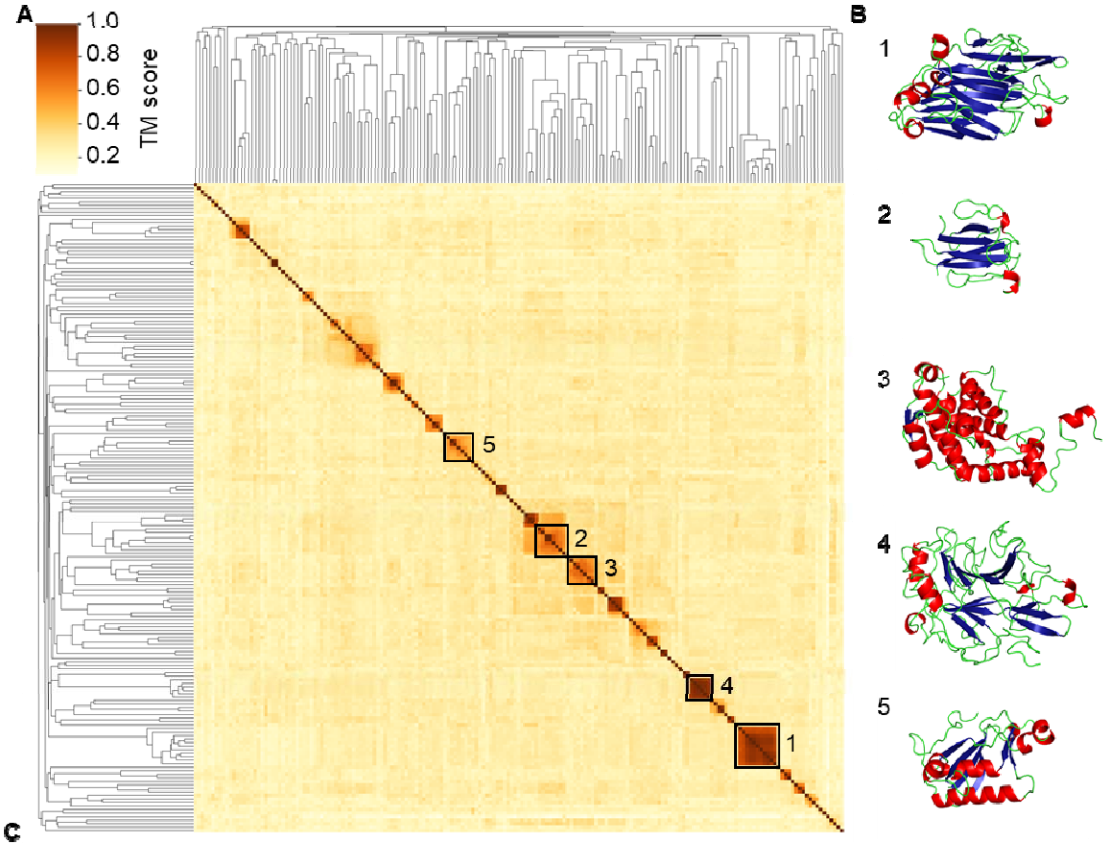

Cluster	Effector proteins	Average TM-score	Average Sequence identity	Annotation
1	11	0,85	43,47 %	Dehydrogenases
2	8	0,63	17,46 %	Glycoside hydrolases
3	7	0,64	21,27 %	Small secreted proteins
4	6	0,91	46,71 %	Cyanamide hydratases
5	6	0,57	18,29 %	Glucanosyl-transferases

315

316 **Figure 4. *R. necatrix* effector candidates show weak structural clustering,**
317 **which is based on sequence conservation.** (A) Ordered by hierarchical clustering
318 based on structural similarity, the heatmap displays the structural similarity of each
319 effector pair in an all-vs-all alignment based on template modelling (TM) scores that
320 range from 0 to 1. Effector clusters were identified based on a similarity threshold >
321 0.5. The five largest clusters are highlighted with a black square and ordered by size.
322 (B) Example structure for each of the five clusters based on the effector with the
323 highest similarity to other effectors in the cluster. (C) Characteristics of the five
324 largest structural effector clusters.

325

326 **Antimicrobial activity in culture filtrates**

327 It has recently been proposed that fungal plant pathogens employ effectors with
328 antimicrobial activity to manipulate the host microbiota to promote infection
329 (Rovenich et al., 2014; Wilson and McDowell, 2022; Snelders et al., 2022). To
330 explore if the soil-borne fungus *R. necatrix* potentially exploits antimicrobials, we
331 first tested whether *R. necatrix* culture filtrates can inhibit the growth of plant-
332 associated bacteria. To this end, we collected *R. necatrix* culture medium after 4,
333 7 and 9 days of fungal growth by filtration through a 0.45 nm filter, and an
334 aliquot of each of the culture filtrates was heat-inactivated at 95°C for 10
335 minutes. Finally, the culture filtrates were used as growth medium for individual
336 bacterial species from a diversity panel of 37 plant-associated bacteria
337 (Supplemental Table 3). After overnight incubation, growth of four of the 37
338 bacteria was inhibited in the 4- and 7-day culture medium filtrates when
339 compared with cultivation in the heat-inactivated culture filtrates, namely
340 *Bacillus drentensis, Achromobacter denitrificans, Sphingobium mellinum* and
341 *Flavobacterium hauense.* While three of these were not found to be inhibited
342 anymore in the 9-day culture medium filtrate, growth of *B. drentensis* was also
343 still inhibited in this filtrate (Fig. 5). Collectively, these findings suggest that the
344 culture medium of *R. necatrix* contains (a) heat-sensitive molecule(s) with
345 selective antimicrobial activity.

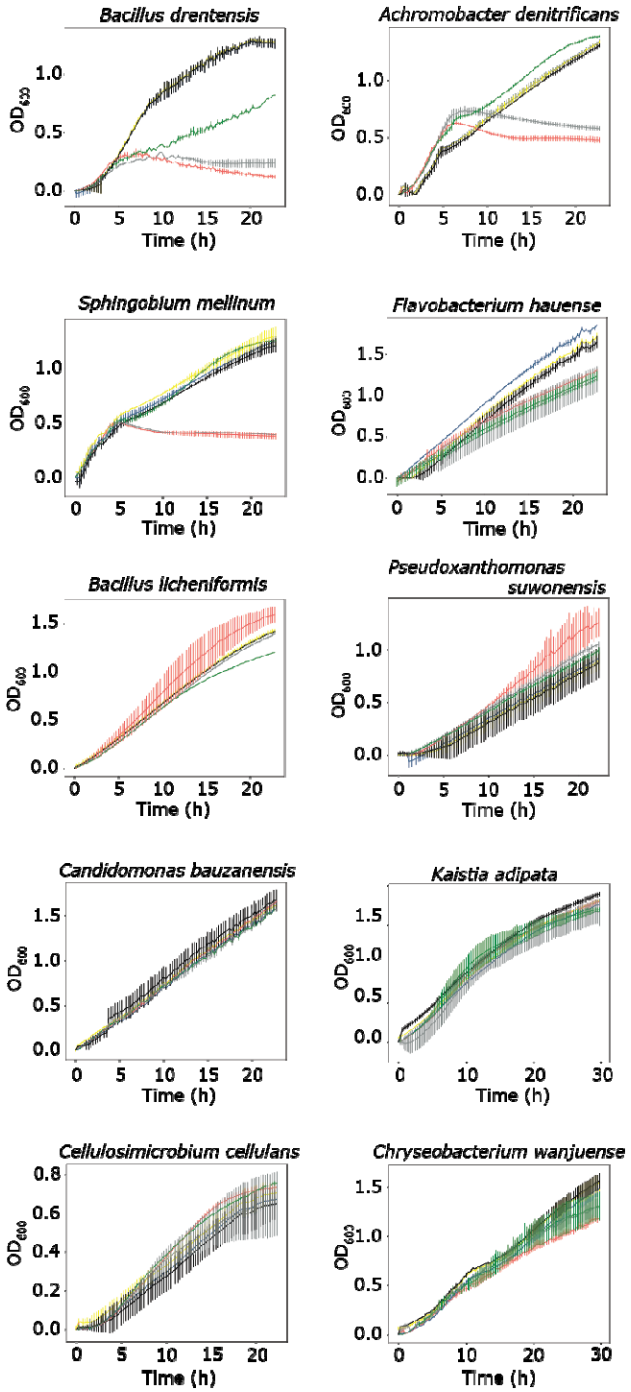

346

347

348 **Figure 5. *Rosellinia necatrix* culture filtrates inhibit the growth of particular**
349 **plant-associated bacterial species.** Bacterial growth was measured over time in
350 *R. necatrix* culture filtrates, which were obtained after 4 (red), 7 (grey) and 9
351 (green) days of fungal growth. Heat-inactivated culture filtrates collected after 4
352 (blue), 7 (yellow) and 9 (black) days of fungal growth were used as controls.

353 **Table 3. Predicted secreted proteins of *R. necatrix* strain R18 with**
354 **structural homology to known antimicrobial proteins.**

***R. necatrix* gene ID**	**Structural homolog[a]**	**Prediction confidence (%)**	**Alignment coverage (%)[b]**	**Homolog protein size (kDa)[c]**	**Cys (%)[d]**	**pI[e]**
FUN_000307	Bacterial enterotoxin	38,6	14	22.2	2.8	4.86
FUN_000408	Toxin	100	64	40.7	3.8	5.68
FUN_000625	Peptidoglycan-binding	100	98	12.3	4.5	8.79
FUN_000907	Toxin	40,1	35	28	2.6	5.03
FUN_001825	Hydrolase	100	95	38.4	1.8	5.11
FUN_001865	EGF/Laminin	91,4	13	34.6	3.6	7.01
FUN_002055	Endoglucanase	100	89	28.6	5.9	6.73
FUN_003304	Hydrolase	100	96	39.2	2.4	5.68
FUN_003451	Fungal ribonucleases	100	92	14.7	3.6	4.19
FUN_004580	Antifungal protein AFP1	55,5	6	47	2.5	4.85
FUN_004961	Toxin	25,2	23	19.7	3.8	7.75
FUN_005431	Thermolabile hemolysin	100	99	32.4	0.8	4.36
FUN_005483	NLP	100	87	28.9	3.3	4.87
FUN_005751	Fungal ribonuclease	100	93	14.4	3.6	6.05
FUN_005940	Toxin	40,6	17	13.9	5.8	6.63
FUN_006760	Carboxypeptidase	100	92	60.9	1.5	5.11
FUN_007808	Toxin	100	55	89	5.8	5.36
FUN_007991	Toxin	45,1	26	19	2.6	9.00
FUN_008352	Toxin	100	99	16.9	6.2	6.14
FUN_009115	Antimicrobial MIAMP1	87,8	33	24	3.2	4.65
FUN_009151	Phage lysozyme	100	94	20.7	3.6	6.92
FUN_009266	Neutrophil defensin 4	44,9	10	15.6	3.3	7.59
FUN_010039	Toxin	100	99	17.0	4.5	6.73
FUN_010165	Toxin	50,3	11	17.5	5.8	4.83
FUN_011519	Antimicrobial protein	15,2	57	5.8	5.7	4.78
FUN_011592	Defensin	49,9	10	18.8	6.7	7.41

355 [a]Structural homology was determined based on Phyre2 prediction (Kelley et al., 2015).
356 [b]Alignment coverage of the *R. necatrix* gene query to the database homolog (subject).
357 [c]Protein size expressed in kilodaltons (kDa) of the database homolog.
358 [d]Amount of cysteines (Cys) present in the database homolog expressed in percentage (%).
359 [e]Isoelectric point (pI) of the database homolog.
360

361 **Prediction of potential antimicrobial effector candidates**

362 We previously showed that structural prediction successfully identified
363 antimicrobial effector proteins encoded in the genome of *V. dahliae* (Snelders et
364 al., 2020; 2021). Thus, we similarly mined the secretome of the *R. necatrix*
365 strain R18 for structural homologues of known antimicrobial proteins using
366 Phyre2 (Snelders et al., 2020; Kelley et al., 2015), leading to the identification of
367 26 candidates with potential antimicrobial activity (Table 3). Subsequently, we
368 used publicly available RNAseq data (Shimizu et al., 2018) to asses expression of
369 these candidates and found that nine of the 26 candidates are highly expressed
370 during avocado colonization (Fig. 6A). To further asses *in planta* expression of
371 the nine candidates, we measured their expression in *R. necatrix* strain R18 upon
372 cotton inoculation, revealing that five genes are highly expressed during cotton
373 colonization (Fig. 6B). To test whether these *in planta*-expressed secreted
374 proteins indeed possess antimicrobial activity, we pursued heterologous protein
375 production in *E. coli*. Unfortunately, we repeatedly failed to produce four of these
376 proteins (FUN_009266, FUN_0100039, FUN_005751 and FUN_006760) which,
377 although it may be interpreted as a sign of potential antimicrobial activity
378 (Ingham and Moore, 2007), obstructs functional analysis. However, one protein
379 could be successfully produced and purified (FUN_004580).

380 FUN_004580 has predicted structural homology to antifungal protein 1
381 (AFP1) from the bacterium *Streptomyces tendae* (Campos-Olivas et al., 2001)
382 (Fig. 7A). This protein was identified in a screen for antifungal activity as a non-
383 enzymatic chitin-binding antifungal directed against particular Ascomycete fungi
384 (Bormann et al., 1999). Intriguingly, attempts to produce functional AFP1 in the
385 lactic acid bacterium *Lactococcus lactis* failed (Freitas et al., 2005), suggesting
386 that the protein may exert antibacterial activity as well. BLAST searches using

387 the FUN_004580 amino acid sequence revealed ~100 Ascomycete fungal
388 homologs, while HMMER searches revealed homologs in the Streptophyta clade
389 (Viridiplantae) too (Supplemental Table 5). Interestingly, BLAST and HMMER
390 searches using the amino acid sequence of FUN_004580 did not reveal homology
391 to AFP1, underpinning that structural homology, rather than sequence homology,
392 drove the prediction of FUN_004580 as an antimicrobial.

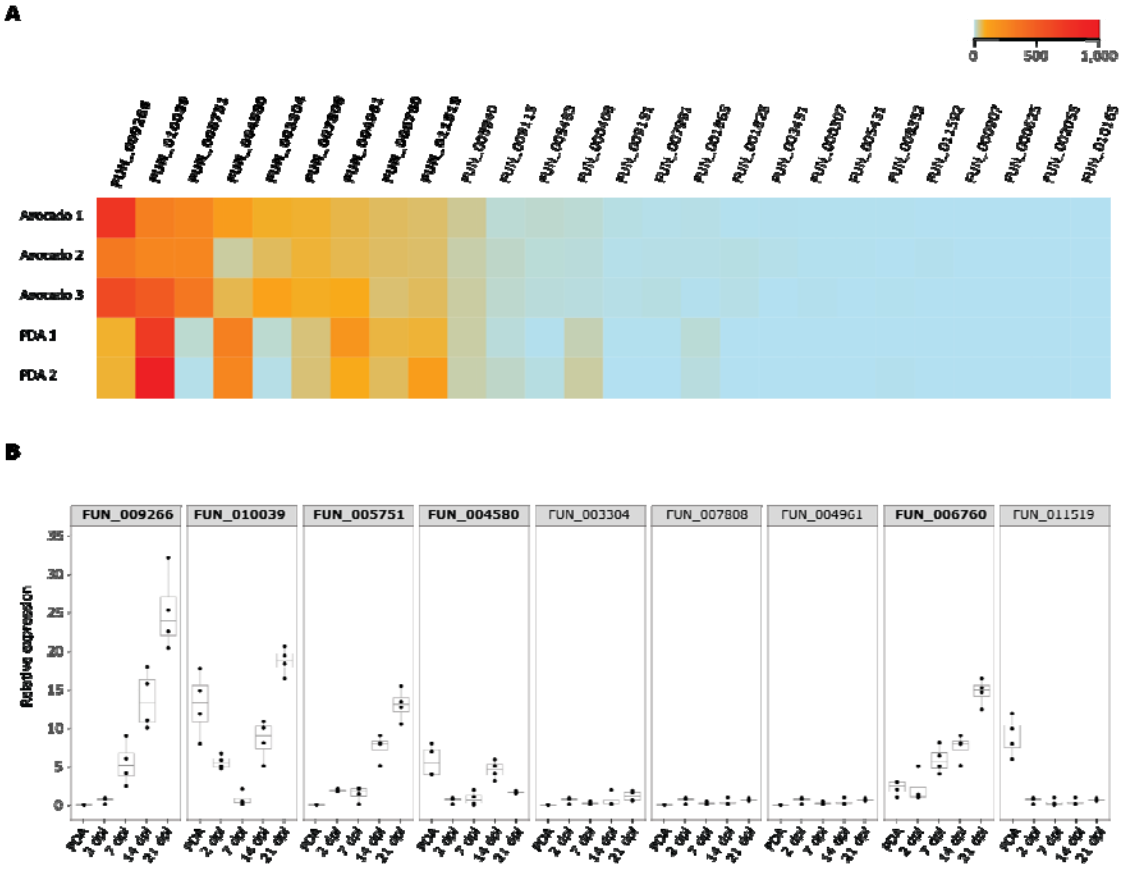

393

394 **Figure 6. *In planta* expression of *Rosellinia necatrix* genes predicted to**
395 **encode effector proteins with antimicrobial activity.** (A) *In silico* analysis of
396 publicly available RNAseq data of avocado plants infected with *R. necatrix* (n=3)
397 reveals nine genes that are highly induced *in planta* (shown in bold) out of 26 that
398 encode potential antimicrobial proteins (AMPs). Several of these are also expressed
399 upon cultivation of *R. necatrix in vitro* on potato dextrose agar (PDA) (n=2). (B)
400 Real-time PCR of nine *in planta* expressed *R. necatrix* genes identified in (A) reveals
401 that five genes are expressed during cotton colonization at 14 and 21 days post
402 inoculation (shown in bold).

403

404 An alternative manner to obtain proteins for functional analysis that does
405 not rely on expression in heterologous microbial expression systems is peptide
406 synthesis, although this is typically limited to sequences shorter than 100 amino
407 acids. Unfortunately, all five effectors that are expressed in cotton are larger
408 than this size. However, among the nine candidates that are highly expressed
409 during avocado colonization, one encodes a protein (FUN_011519) small enough
410 for protein synthesis (Biomatik Corporation, Ontario, Canada).

411 FUN_011519 has predicted structural homology to the antimicrobial
412 protein AcAMP2 from the plant *Amaranthus caudatus* (Martins et al., 1996) (Fig.
413 7B). This protein was identified based on homology to cysteine/glycine-rich
414 domain of plant chitin-binding proteins and showed antifungal activity, as well as
415 activity against Gram-positive bacteria (Broekaert et al., 1992). BLAST and
416 HMMER searches revealed only Ascomycete fungal homologs, identifying ~100
417 fungal proteins (Supplemental Table 6). Interestingly, BLAST and HMMER
418 searches using the amino acid sequence of FUN_011519 did not reveal homology
419 to AcAMP2, underpinning that also in this case structural homology, rather than
420 sequence homology, drove the prediction as antimicrobial.

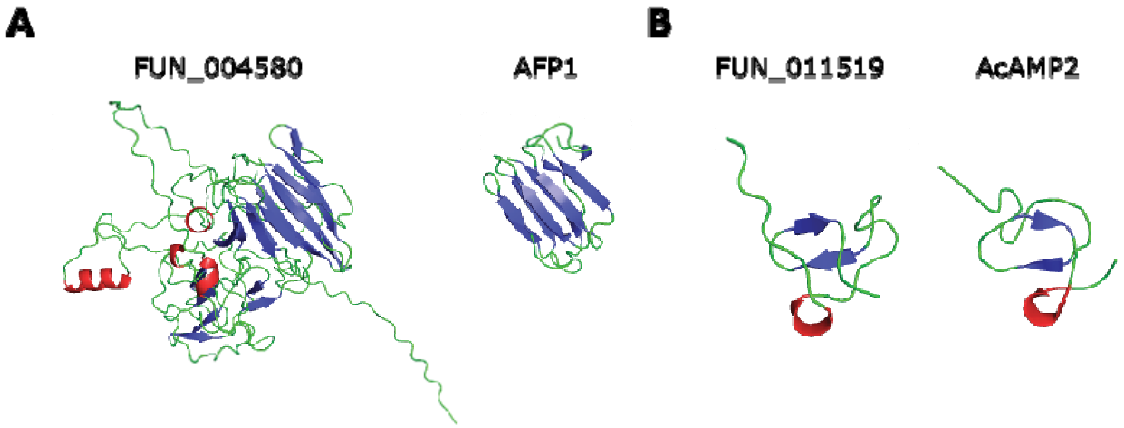

421

422 **Figure 7. *Rosellinia necatrix* effector proteins with predicted antimicrobial**
423 **activity based on structural homology.** (A) Alphafold2 model of *R. necatrix*
424 effector protein FUN_004580 (left) shows structural homology to antifungal protein
425 1 (AFP1) from the bacterium *Streptomyces tendae* (right). (B) Alphafold2 model

426 of *R. necatrix* effector protein FUN_011519 (left) shows structural homology to
427 antimicrobial protein AcAMP2 from the plant *Amaranthus caudatus* (right).

428

429 **Candidate antimicrobial effector proteins display selective antimicrobial**
430 **activity**

431 Given that FUN_004580 and FUN_011519 were identified based on structural
432 homology to proteins with antifungal activity, we tested potential antimicrobial
433 activity on eight fungal species: four filamentous fungi (*Verticillium dahliae*,
434 *Alternaria brassicicola*, *Cladosporium cucumerinum* and *Trichoderma viridae*),
435 and four yeasts (*Pichia pastoris*, *Cyberlindnera jadinii*, *Debaryomyces vanrijiae*
436 and *Rhodorotula bogoriensis*). Interestingly, both proteins displayed selective
437 antifungal activity. Whereas FUN_004580 inhibited the growth of all filamentous
438 fungi tested (Fig. 7A) as well as of all yeasts except *P. pastoris* (Fig. 7B),
439 FUN_011519 had a narrower activity spectrum as it only inhibited the growth of
440 *V. dahliae* and *A. brassicicola* (Fig. 7C), and the yeasts *C. jadinii* and *R.*
441 *bogoriensis* (Fig. 7D). Thus, we conclude that both proteins possess clear
442 antifungal activity.

443 To further investigate the antimicrobial activity of the two effector proteins
444 FUN_004580 and FUN_011519, we tested their activity on the diversity panel of
445 37 bacteria that span a wide range of taxonomic diversity, including Gram-
446 positive and Gram-negative taxa (Table 5). Interestingly, although we found that
447 the growth of most bacteria was not affected by any of the two proteins, growth
448 of some bacteria was clearly hampered. Whereas FUN_004580 strongly impacted
449 growth of *Pseudoxanthomonas suwonensis*, *Flavobacterium hauense*, and
450 *Cellulosimicrobium cellulans*, and inhibited *Chryseobacterium wanjuense* to a
451 lesser extent, FUN_011519 inhibited *Bacillus drentensis* and *Achromobacter*
452 *denitrificans*, and possibly also *Sphingobium mellinum* and *Candidimonas*

453 *bauzanensis* (Fig. 8). Thus, we conclude that both effectors display antibacterial
454 activity as well. Collectively, our data show that both effector proteins possess
455 selective antimicrobial activity.

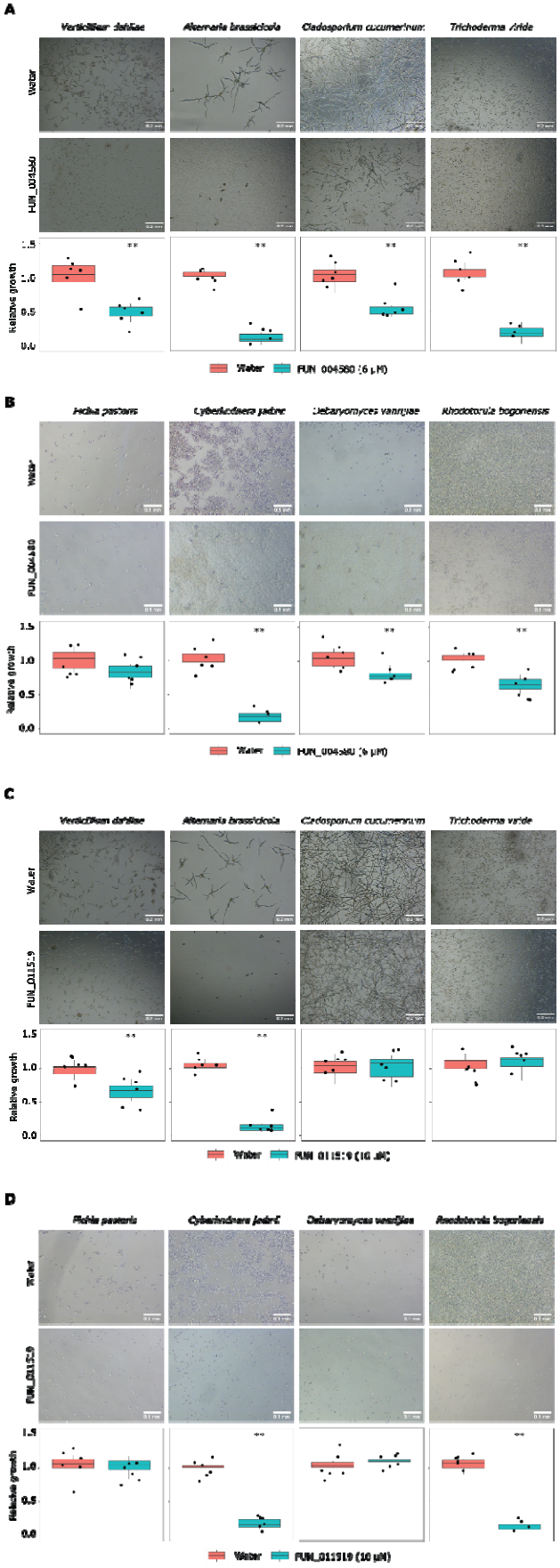
A
Alternaria brassicicola
Cladosporium cucumerinum
Trichoderma viride
Water
Relative growth
Water
B
Pichia pastoris
Rhodotorula bogoriensis
Water
Relative growth
Water
C
Alternaria brassicicola
Cladosporium cucumerinum
Trichoderma viride
Water
Relative growth
Water
D
Pichia pastoris
Water
Relative growth
Water

457 **Figure 8. *Rosellinia necatrix* effector proteins display antifungal activity.**
458 Fungal growth in 5% potato dextrose broth (PDB) in presence of FUN_004580 (6 µM)
459 or water of filamentous fungal species (A) and yeasts (B), or in presence of
460 FUN_011519 (10 µM) or water of filamentous fungal species (C) and yeasts (D).
461 Relative growth as display in microscopic pictures (n=6) was quantify using ImageJ.
462 Asterisks indicate significant differences (unpaired two-sided Student's t test
463 (P<0.01)).

464

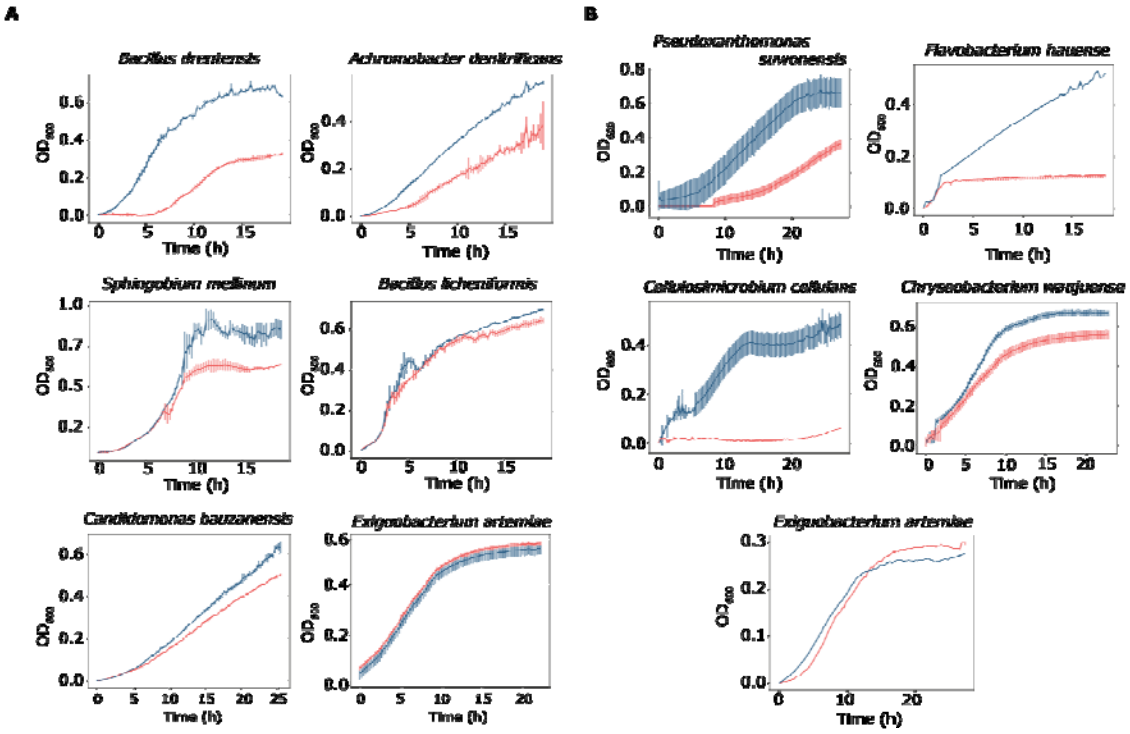

465

466 **Figure 9. *Rosellinia necatrix* effector proteins display selective antimicrobial**
467 **activity against plant-associated bacteria.** (A) Red lines show bacterial growth in
468 presence of FUN_011519 (10 µM) while blue lines show bacterial growth in water.
469 (B) Red lines show bacterial growth in presence of FUN_004580 (6 µM) while blue
470 lines show bacterial growth in water. Error bars display standard deviations (n=3).
471 Growth of *Exiguobacterium artemiae* is not inhibited by either protein and is shown
472 as a representative of non-inhibited bacterial taxa.

473

474 **Several plant-associated bacteria display antagonistic activity**

475 One obvious reason for a fungus to target particular microbes with antimicrobials
476 is that these may be detrimental to fungal growth due to the display of
477 antagonistic activities. To test for such activities directed against *R. necatrix*, we
478 conducted confrontation assays *in vitro*, where we grew *R. necatrix* near the

479 individual bacteria species from the diversity panel of 37 bacteria (Table 5). In
480 these assays, we observed antagonistic effects of several bacterial strains on *R.*
481 *necatrix* (Fig. 9). Interestingly, several of the bacterial species inhibited by either
482 of the two effector proteins displayed antagonistic activity against *R. necatrix*,
483 including *Bacillus drentensis*, *Bacillus licheniformis*, and *Sphingobium mellinum*
484 (inhibited by FUN_011519), and *Cellulosimicrobium cellulans*, *Chryseobacterium*
485 *wanjuense* and *Pseudoxanthomonas suwonensis* (inhibited by protein
486 FUN_004580) (Fig. 8). However, also some other bacterial species that were not
487 found to be inhibited by either of the two effector proteins displayed antagonistic
488 activity, namely *Kaistia adipata, Pedobacter steynii, Pedobacter panaciterrae,*
489 *Pseudomonas corrugata, Pseudomonas knackmusii, Solibacillus isronensis* and
490 *Solibacillus silvestris*. These findings suggest that a diversity of plant-associated
491 bacteria possess inherent antagonistic activity against *R. necatrix* and that some
492 of these bacteria are targeted by effector proteins of *R. necatrix.*
493

494 **Particular antagonists alleviate Rosellinia disease in cotton**

495 To test whether any of the bacterial strains that are inhibited by the *R. necatrix*
496 effector proteins and that display antagonistic activity against the fungus can
497 promote the suppression of disease development, we pursued inoculation assays
498 in the presence and absence of these bacteria. As *R. necatrix* is a broad host
499 range pathogen, we performed infection assays on cotton plants. To this end,
500 14-day-old cotton cv. XLZ seedlings were inoculated with *R. necatrix* strain R18,
501 leading to clear disease symptoms by two weeks after inoculation (Fig. 10).
502 Next, we pre-treated cotton cv. XLZ seeds with *Bacillus drentensis, Sphingobium*
503 *mellinum, Cellulosimicrobium cellulans* or *Pseudoxanthomonas suwonensis*,
504 followed by *R. necatrix* inoculation. Interestingly, two weeks after inoculation it

505 could be observed that pretreatment with each of the bacteria resulted in
506 reduced susceptibility of the cotton plants to *R. necatrix* when compared with the
507 plants that did not receive a bacterial pre-treatment, while none of the bacteria
508 affected growth of the cotton plants in absence of pathogen inoculation (Fig. 10).

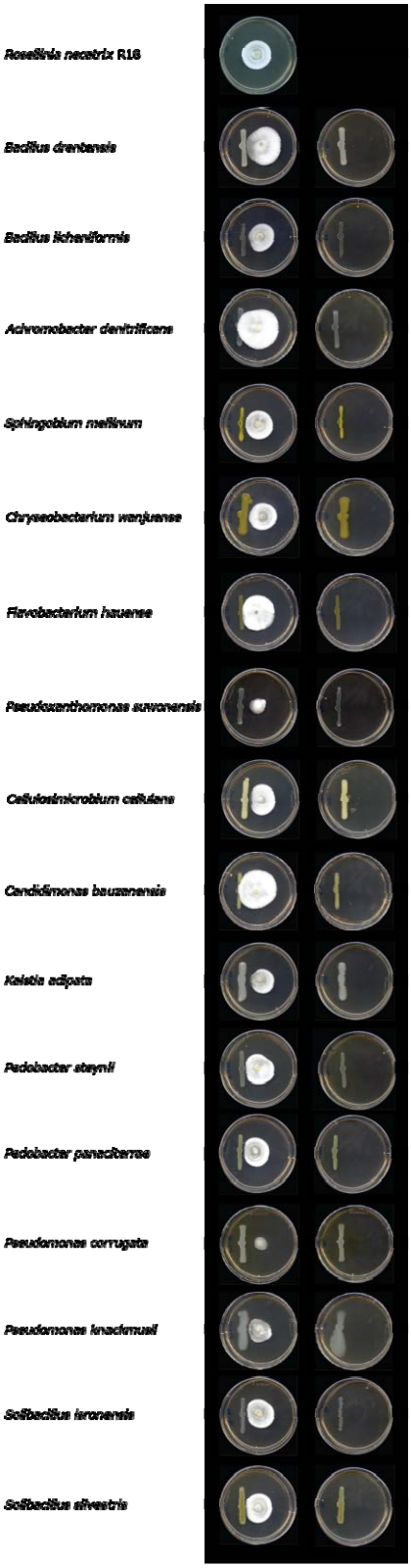

Figure 10. **Various plant-associated bacteria display antagonistic activity against R*osellinia necatrix*.** Fungal PDA disks were placed in the center of a petri dish and next to it individual bacteria species were deposited in a straight line with help of a spreader (n=5).

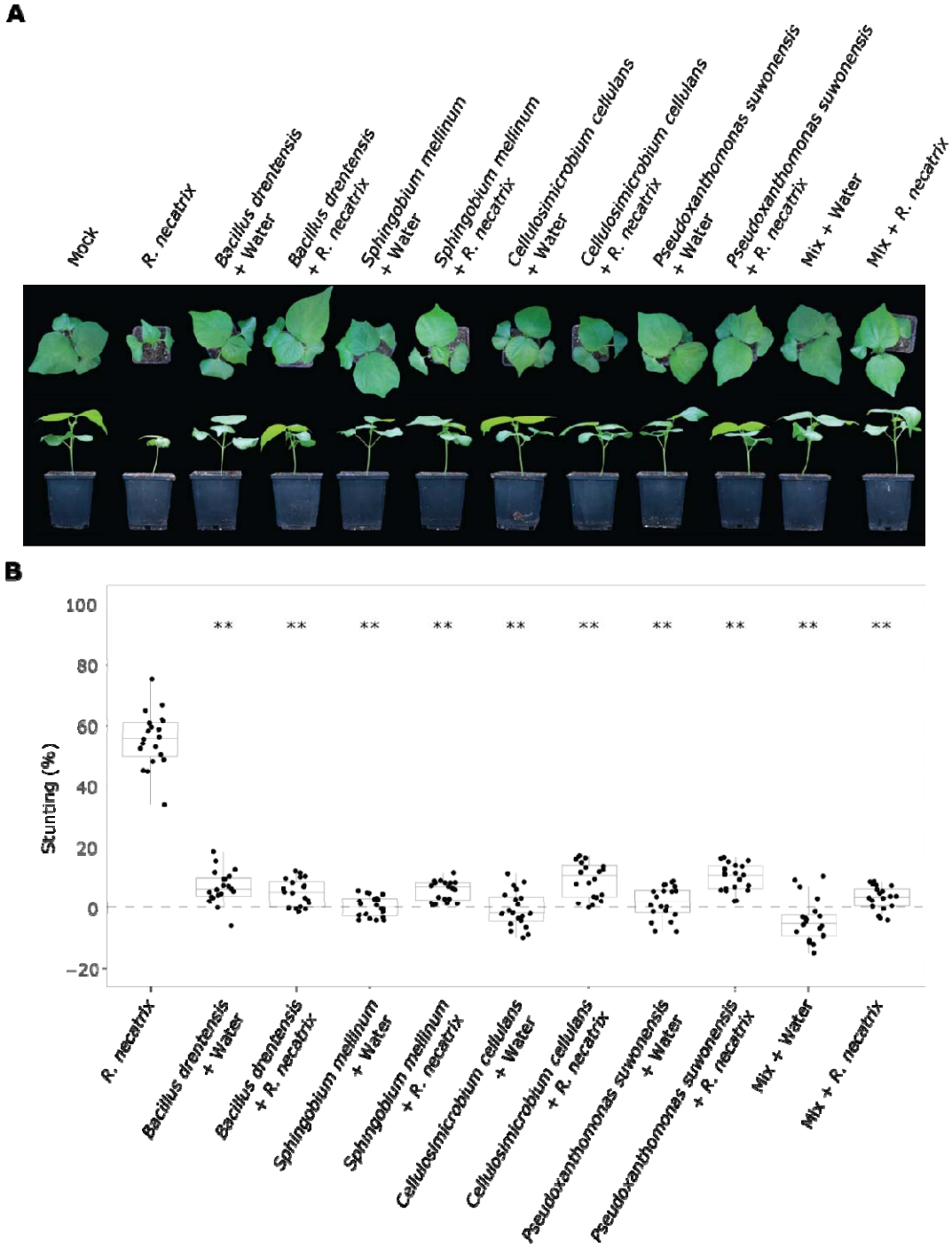

514

515 **Figure 11**. **Antagonistic plant-associated bacteria reduce white root rot**
516 **disease in cotton.** (A) Top and side pictures of cotton plants. Cotton seeds were
517 soaked in a suspension of the antagonistic bacteria *Bacillus drentensis*, *Sphingobium*
518 *mellinum*, *Cellulosimicrobium cellulans*, or *Pseudoxanthomonas suwonensis*, or water
519 as a control. Subsequently, germlings (n=20) were inoculated with *R. necatrix* strain
520 R18 or mock-inoculated. (B) Quantification of stunting. Asterisks indicate significant
521 differences between *R. necatrix*-inoculated plants and plant seeds treated with
522 bacteria (ANOVA followed by Fisher's LSD test ($P<0.01$)).

523 **DISCUSSION**

524 Increasing evidence supports the notion that plants can recruit microbes into
525 their microbiota that can help them to withstand pathogen infection (Wang et al.,
526 2012; Pérez-Jaramillo et al., 2016; Zhalnina et al., 2018; Chai and Schachtman,
527 2022). Based on this notion, it has been hypothesized that pathogens have
528 evolved to counter-act the recruitment of beneficial microbes to promote host
529 colonization (Snelders et al., 2018). In support of this hypothesis, it has been
530 shown that the soil-borne fungal pathogen *Verticillium dahliae* secretes a suite of
531 effector molecules with selective antimicrobial activities to suppress antagonistic
532 microbes in host microbiota to support host ingress (Snelders et al. 2020; 2021;
533 2022). Although it has been hypothesized that other fungal pathogens are likely
534 to have evolved to modulate host microbiota as well (Snelders et al. 2020;
535 Snelders et al. 2022), evidence for this hypothesis has been lacking thus far. In
536 this study, we show that the soil-borne pathogen *Rosellinia necatrix* similarly
537 secretes effector proteins during host colonization that possess selective
538 antimicrobial activity. Specifically, we show that two effector proteins,
539 FUN_004580 and FUN_011519, are secreted during host colonization and display
540 selective antimicrobial activity *in vitro* towards a specific plant-associated
541 bacteria and fungi. Intriguingly, some of the bacterial species that are inhibited
542 by the antimicrobial effector proteins display antagonistic activity towards *R.*
543 *necatrix in vitro*. Moreover, when applied to cotton seeds, several of the
544 antagonistic bacterial species reduce white root rot disease. Collectively, our
545 findings suggest that *R. necatrix* secretes antimicrobial effector proteins during
546 host colonization to modulate host microbiota and support disease development.

547 The effector proteins FUN_004580 and FUN_011519 showed selective
548 antimicrobial activity against plant-associated bacterial and fungal species *in*

549 *vitro* and display divergent activity spectra, suggesting that they complement
550 each other in their activities. Similar observations have been made for the
551 antimicrobial effector proteins VdAMP2 and VdAve1 of *V. dahliae* that
552 complement each other during soil colonization (Snelders et al., 2020). Similarly,
553 also the *in planta*-expressed effectors VdAve1, VdAve1L2 and VdAMP3 display
554 divergent activity spectra (Snelders et al., 2020; 2022). Furthermore, differential
555 expression of antimicrobial effectors on different plant hosts was observed in *R.*
556 *necatrix*. Out of the 26 AMP candidates, nine are expressed during avocado
557 colonization, and five of them were also expressed during cotton colonization.
558 From these, *FUN_004580* and *FUN_011519* are expressed during avocado
559 colonization, while only *FUN_004580* is expressed on cotton (Fig. 4). The
560 expression profiles on different host plants suggest differential expression of
561 antimicrobials in *R. necatrix*, potentially due to differential microbiota
562 compositions of these plant hosts. Possibly, FUN_011519 evolved to target
563 microbes that are specifically associated with avocado, or absent from the
564 microbiota of cotton plants.

565 Various studies have shown that plants shape their microbiota composition
566 (Berendsen et al., 2012). For example, one single gene responsible for the
567 production of glucosinolate significantly altered the microbial community on the
568 roots of transgenic *Arabidopsis* (Bressan, 2009). Moreover, the ATP-binding
569 cassette (ABC) transporter *abcg30* mutant of *Arabidopsis thaliana* secretes root
570 exudates that are enriched in phenolic compounds and contain fewer sugars,
571 resulting in distinct root microbiota compositions (Badri and Vivanco, 2009).
572 Furthermore, *A. thaliana* genes responsible for defense, kinase-related activities,
573 and cell wall integrity impact the microbiota composition (Beilsmith et al., 2019).

574 Besides *A. thaliana*, different potato and tomato plants assemble different
575 microbiota compositions (Weinert et al., 2011; Cordovez et al., 2021).

576 Like *V. dahliae*, *R. necatrix* is a soil-borne pathogen that resides for part of
577 its life cycle in the microbe-rich soil where inter-microbial competition for limited
578 nutrients is ferocious. Although *R. necatrix* is phylogenetically related to *V.*
579 *dahliae*, both belonging to the class of Sordariomycetes, our findings suggest
580 that exploitation of antimicrobial effector proteins among soil-borne fungi may be
581 commonplace. However, whether the employment of such effector proteins is
582 relevant for soil-borne pathogens only, or shared by other types of plant
583 pathogens too, presently remains enigmatic (Snelders et al., 2022a).

584 To further investigate the effector catalog of *R. necatrix*, we investigated
585 whether effector genes in *R. necatrix* are associated with repetitive regions. The
586 genomes of many filamentous plant pathogens are compartmentalized,
587 comprising gene-dense/repeat-poor regions harboring essential and widely
588 conserved housekeeping genes and gene-sparse/repeat-rich regions containing
589 fast-evolving virulence-associated genes (Rafaelle et al., 2010; Dong et al.,
590 2015; Frantzeskakis et al., 2020). However, in the case of *R. necatrix*, the repeat
591 content is low, and interestingly, the vast majority of repetitive elements are not
592 located in close proximity to effectors. This suggests that effector genes in *R.*
593 *necatrix* are not associated with repeat-rich regions. Similar to *R. necatrix*, other
594 genomes have been found to lack obvious genome compartmentalization, such
595 as the barley powdery mildew fungus *Blumeria graminis* f.sp. *hordei*
596 (Frantzeskakis et al., 2018) and the wheat stripe rust fungus *Puccinia striiformis*
597 f.sp. *tritici* (Schwessinger et al., 2018). In these cases, adaptation and evolution
598 of effector genes were suggested to be governed by copy-number variation
599 (CNV) and heterozygosity of the effector loci (Frantzeskakis et al., 2018). In *R.*

600 *necatrix,* we showed that insertions and deletions are predominant structural
601 variants (SVs) that are associated with effector genes, which suggests that these
602 SVs may play a role in evolution of the effector catalog.

603 To understand the diversity and functional properties of effectors, we
604 investigated their 3D protein structure. The results of this study demonstrate
605 that there is relatively little structural clustering among *R. necatrix* effectors. The
606 five largest clusters identified were mainly driven by sequence conservation
607 rather than structural similarity, suggesting that effector family expansion played
608 only a minor role in *R. necatrix* effector evolution. Effector protein structure
609 clustering has revealed that many plant pathogen effectors fall into distinct
610 structural families. For example, MAX (de Guillen et al., 2015), and RNase-Like
611 proteins associated with haustoria (RALPH) (Spanu, 2017) are effector families
612 with structural similarity. Common themes are emerging like structural homology
613 and in some cases similar modes of action (Lu et al., 2015). While structural
614 conservation has been observed in some pathogenic fungi (de Guillen et al.,
615 2015; Spanu, 2017), sequence conservation is the main driver of structural
616 clustering among *R. necatrix* effectors. Future studies could explore the
617 functional significance of the identified effector clusters in *R. necatrix* and other
618 plant pathogens and investigate the mechanisms underlying the evolution of
619 effector proteins.

620 **MATERIALS AND METHODS**

621 **Nanopore sequencing and genome assembly**

622 High-molecular weight (HMW) DNA was extracted from nine *R. necatrix* strains
623 (Table 1) as described by Chavarro-Carrero et al. (2021), except that mycelium
624 was grown in 1/5 PDB instead of Czapek Dox medium. DNA quality, size and
625 quantity were assessed with Nanodrop, Qubit analyses, and with gel
626 electrophoresis. Library preparation with the Rapid Sequencing Kit (SQK-
627 RAD004) was performed with ~400 ng HMW DNA according to the
628 manufacturer's instructions (Oxford Nanopore Technologies, Oxford, UK). An
629 R9.4.1 flow cell (Oxford Nanopore Technologies, Oxford, UK) was loaded and ran
630 for 24 h, and subsequent base calling was performed using Guppy (version
631 3.1.3; Oxford Nanopore Technologies, Oxford, UK). Adapter sequences were
632 removed using Porechop (version 0.2.4 with default settings; Wick, 2018) and
633 the reads were self-corrected, trimmed and assembled using Canu (version 1.8;
634 Koren et al., 2017).

635 To obtain longer reads ultra-high-molecular weight (UHMW) DNA
636 extraction was performed. To this end, after DNA precipitation, the Nanobind Big
637 DNA Kit (SKU NB-900-801-01, Circulomics, USA) was used following the
638 manufacturer's protocol to select DNA fragments >50 kb. Simultaneously, to
639 allow error correction of the ONT reads, paired-end short read (150 bp)
640 sequencing was performed at the Beijing Genome Institute (BGI) using the
641 DNBseq platform. After error correction using FMLRC (version 1.0.0 with default
642 settings; Wang et al., 2018), ONT reads were trimmed and assembled using
643 Canu.

644 Hi-C was performed based on the Proximo Hi-C kit (Microbe) (Phase
645 Genomics, Seattle, WA, USA) according to the manufacturer's protocol as

646 previously described (Seidl et al., 2020), and the Hi-C library was paired-end
647 (150 bp) sequenced on the NextSeq500 platform at USEQ (Utrecht, the
648 Netherlands). Subsequently, Hi-C reads were mapped to the Canu assembly
649 using Juicer (version 1.6 with early-stage setting; Durand et al., 2016), and the
650 three-dimensional (3D) *de novo* assembly (3D-DNA) pipeline (version 180922
651 with contig size threshold 1000; Dudchenko et al., 2017) was used. The genome
652 assembly was further manually improved using Juicebox Assembly Tools (JBAT)
653 (version 1.11.08; Dudchenko et al., 2018) and the 3D-DNA post review asm
654 pipeline (Dudchenko et al., 2017). Tapestry (version 1.0.0 with default settings;
655 (Davey et al., 2020) was used to visualize chromosomes and telomeric regions
656 with telomeric sequence ([TTAGGG]*n*).
657

658 **Phylogenetic tree construction and structural variant calling**

659 A phylogenetic tree of all sequenced strains was constructed with Realphy
660 (version 1.12) (Bertels *et al.,* 2014). Briefly, genomic reads were mapped
661 against the genome of strain R18 using Bowtie2 (version 2.2.6) (Langmead and
662 Salzberg, 2012) and a maximum-likelihood phylogenetic tree was inferred using
663 RAxML (version 8.2.8) (Stamatakis, 2014), using the genome sequence of
664 *Rosellinia corticium* to root the tree. Subsequently, to predict SVs, we used
665 NanoSV (version 1.2.4 with default settings; Stancu et al., 2017) for each of the
666 genomes when compared to R18 strain as reference. The output of each strain
667 was initially filtered with bcftools v.1.3.2 using GT=AA, QUAL>50, GQ>10,
668 SUPPORT>20 (Danecek et al., 2021). The results were merged using SURVIVOR
669 v.1.0.6 (Jeffares et al., 2017), allowing 1,000 bp as the maximum distance for
670 breakpoints and considering only same SV types. Only SVs with minimum size
671 >100 bp and maximum size of 100 kb were kept. Permutation tests were

672 computed using R/Bioconductor region v.1.8.1 package (Gel et al., 2016), and
673 10,000 iterations were performed using the mean distance to evaluate the
674 closest relationship (bp distance) between SV-breakpoints, TEs and effectors,
675 and circular randomization as well to maintain the order and distance of the
676 regions on the chromosomes.
677
678 **Genome mining**
679 Genome annotation was performed using Funannotate (Version 1.8.13, Palmer
680 and Stajich, 2017) guided by publicly available RNAseq data (Shimizu et al.,
681 2018). Furthermore, secreted genes, effector genes and secondary metabolite
682 gene clusters were predicted using SignalP (Version 5.0, Almagro et al., 2019),
683 EffectorP (Version 2.0, Sperschneider et al., 2018) and antiSMASH (Version
684 6.0.0, Blin et al., 2019), respectively. The *R. necatrix* R18 genome was mined for
685 gene candidates that encode secreted antimicrobials as described previously
686 (Snelders et al., 2020). Briefly the predicted secretome and effector catalog were
687 mined using Phyre2 (Kelley et al., 2015), followed by manual curation, to search
688 for predicted structural homologues of known antimicrobial proteins. Gene
689 sequences were extracted using Bedtools (setting: getfasta) (Quinlan and Hall,
690 2010). Subsequently, RNAseq data were used to confirm expression of selected
691 candidates. To this end, RNAseq data was mapped to the R18 assembly and
692 relative expression was calculated using Kallisto (version 0.46.1, default settings,
693 Bray et al., 2016).
694 Repetitive regions were annotated using EDTA v.1.9.4 (Ou et al., 2019).
695 Briefly, we used the 'sensitive', 'anno' and 'evaluate' options to maximize the
696 transposable element discovery and integrity. Then, the TE library was refined

697 using one code to find them all (Bailly-Bechet et al., 2014), and only full LTRs
698 were kept.
699
700 **Structural prediction of the *R. necatrix* effector catalog**
701 Structural predictions of effector candidates were done based on mature amino
702 acid sequences, lacking signal peptides, with Alphafold2 (Jumper et al., 2021)
703 using the casp14 preset. Five models were generated for each effector candidate,
704 of which the one with the highest pLDDT score was used for further analysis. To
705 assess structural similarity between effector candidates, an all-vs-all alignment
706 was performed using TM-align (Zhang and Skolnick, 2005). Structures were
707 considered similar when the average TM-score of pairwise reciprocal alignments,
708 calculated on a 0-1 scale, was >0.5. Effector clusters were identified by simple
709 agglomerative hierarchical clustering based on structural similarity using SciPy
710 (Virtanen et al., 2020) and a minimum similarity threshold of 0.5. For the five
711 largest clusters the average sequence identity was calculated from a multiple
712 sequence alignment performed with MAFFT on EMBL-EBI (Katoh and Standley,
713 2013). Cluster annotation was performed by generating PANNZER (Törönen and
714 Holm, 2022) annotation for each protein followed by manual curation of a
715 consensus annotation for each cluster. Protein structures were generated with
716 PyMOL (The PyMOL Molecular Graphics System, Version 2.0 Schrödinger, LLC,
717 DeLano Scientific, Palo Alto, CA, USA).
718
719 **Real-time PCR**
720 To determine expression profiles of candidate genes that encode secreted
721 antimicrobials during *R. necatrix* infection of cotton, two-week-old cotton (cv.
722 XLZ) seedlings were inoculated, as previously described (Cazorla et al., 2006),

723 with *R. necatrix* strain R18, and stems were harvested up to 21 dpi.
724 Furthermore, mycelium was harvested from ten-day-old *R. necatrix* strain R18
725 cultures on potato dextrose agar (PDA) plates. Total RNA extraction and cDNA
726 synthesis were performed as previously described (Santhanam et al., 2013).
727 Real time-PCR was performed with primers listed in Supplemental Table 4, using
728 the *R. necatrix* glyceraldehyde-3-phosphate dehydrogenase gene (GAPDH) as
729 endogenous control. The PCR cycling conditions consisted of an initial 95°C
730 denaturation step for 10 min followed by denaturation for 15□s at 95°C,
731 annealing for 30□s at 60°C, and extension at 72°C for 40□cycles.
732

733 **Heterologous protein production**

734 The sequences encoding mature proteins were cloned into vector pET-15b with
735 an N-terminal His6 tag sequence (Novagen, Darmstadt, Germany) (primer
736 sequences, see Supplemental Table 4). The resulting expression vectors were
737 verified by sequencing and used to transform *Escherichia coli* strain BL21. For
738 heterologous protein production, BL21 cells were grown in 2× yeast extract
739 tryptone (YT) medium at 37°C with continuous shaking at 200 rpm until the
740 cultures reached an optical density measurement at 600 nm (OD_{600}) of 2. Protein
741 production was induced with 1 mM isopropyl β-D-1-thiogalactopyranoside (IPTG)
742 at 42°C and shaking at 200 rpm for 2 h. Bacterial cells were pelleted and washed
743 with 50mM Tris HCl and 10% glycerol at pH 8.0. To disrupt cells, they were
744 sonicated three times according to a cycle composed of one second sonication,
745 followed by 0.5 seconds on ice and a one-minute pause. Next, the samples were
746 centrifugated at 16,000g for 10 min. The insoluble pellets were resuspended in
747 30 mL of 6 M guanidine hydrochloride (GnHCl), 10 mM Tris at pH 8.0 and 10 mM
748 β-mercaptoethanol and incubated overnight at room temperature. Next, debris

749 was pelleted by centrifuging at 16,000g for 10 min and the resulting protein
750 solution was transferred to a new tube and filtered step-wise from 1.2 to 0.45
751 µm. Proteins were subsequently purified under denaturing conditions by metal
752 affinity chromatography using a pre-packed HisTrap FF column (Cytiva,
753 Medemblik, The Netherlands) and dialysed (Spectra/Por 3 Dialysis Membrane,
754 molecular weight cut off of 10 kDa; Spectrum Laboratories, Rancho Dominguez,
755 U.S.A) against 20 volumes of 0.01 M BisTris, 10 mM reduced glutathione and 2
756 mM oxidized glutathione at pH 8.0 with decreasing GnHCl concentrations in five
757 consecutive steps of minimum 24 h from 5 M to 1 M for refolding. Finally,
758 proteins were dialysed against demineralized water for 24 h and final
759 concentrations were determined using Qubit (ThermoFisher Scientific, Waltham,
760 U.S.A).
761
762 **Culture filtrate production**
763 *R. necatrix* strain R18 was grown in potato dextrose broth (PDB) at 21°C and
764 130 rpm. Cultures were collected at 4, 7 and 9 days after the start of incubation
765 and mycelium was separated from the culture medium using a 0.45 nm filter.
766 Half of the culture-filtrate was heat-inactivated at 96°C for 10 minutes. Finally,
767 culture filtrates were stored at -20°C until use.
768
769 ***In vitro* antimicrobial activity assays**
770 Growth assays were performed as previously described (Snelders et al., 2020).
771 Briefly, bacterial strains were grown overnight on lysogeny broth agar (LBA),
772 tryptone soya agar (TSA) or R2A agar at 28°C (Table 5). Subsequently, single
773 colonies were selected and grown overnight at 28°C while shaking at 130 rpm in
774 low-salt Luria broth (LB) (NaCl, 0.5 g/L; Tryptone, 10 g/L; Yeast Extract, 5 g/L).

775 Overnight cultures were resuspended to OD_{600}=0.05 in low-salt LB and 100 µL
776 were supplemented with 100 µL of purified effector proteins or culture filtrates to
777 a final OD_{600}=0.025 in clear 96 well flat-bottom polystyrene tissue culture plates
778 (Greiner CELLSTAR®, Sigma, Burlington, U.S.A). Culture plates were incubated in
779 a CLARIOstar plate reader (BMG LABTECH, Ortenberg, Germany) at 25°C with
780 double orbital shaking every 15 minutes and OD_{600} was measured every 15
781 minutes.

782 Filamentous fungal isolates were grown on PDA at 22°C, while for yeasts,
783 single colonies were selected and grown overnight in 5% PDB at 28°C while
784 shaking at 200 rpm. For yeasts overnight cultures were resuspended to
785 OD_{600}=0.01 in fresh 5% PDB supplemented with water, 10 µM FUN_011519 or 6
786 µM FUN_004580. For filamentous fungi, spores were harvested from PDA and
787 suspended in 5% PDB supplemented with 10 µM FUN_011519, 6 µM
788 FUN_004580 or water to a final concentration of 10^4 spores/mL. Next, 200 µL of
789 the fungal suspensions was aliquoted in clear 96-well flatbottom polystyrene
790 tissue-culture plates (Greiner CELLSTAR®, Sigma, Burlington, U.S.A). Plates were
791 incubated at 28°C, and fungal growth was imaged using an SZX10 stereo
792 microscope (Olympus, Tokyo, Japan) with EP50 camera (Olympus, Tokyo,
793 Japan).

794

795 **Microbial confrontation assays**

796 *R. necatrix* was grown on PDA for 14 days and mycelium disks of 5 mm diameter
797 were taken using a biopsy puncher (Kai Europe, Solingen, Germany). Single *R.*
798 *necatrix* disks were placed in the center of a PDA plate and 100 µL (OD_{600}=0.05)
799 of bacterial culture (Table 5), grown overnight in LB medium at 28°C at 130 rpm,

800 was added in proximity of the fungal disk with a spreader (n=5). After seven
801 days, pictures were taken. The experiment was repeated three times.
802
803 **Biocontrol assay**
804 *Bacillus drentensis, Sphingobium mellinum, Cellulosimicrobium cellulans* and
805 *Pseudoxanthomonas suwonensis* were grown overnight at 28°C in low-salt LB
806 while shaking at 130 rpm. Subsequently, the bacterial suspension was pelleted,
807 washed, and resuspended to OD_{600}=0.05 in water. Seeds of cotton cv. XLZ were
808 surface-sterilized with 2% sodium hypochlorite for ten minutes, washed three
809 times with sterile water, and then soaked for ten minutes the bacterial
810 suspension. Next, the seeds were transferred to sterile Petri dishes containing
811 filter paper moistened with each of the bacterial suspension and incubated in
812 darkness at room temperature. Once the seeds germinated, germlings were
813 transferred to potting soil in the greenhouse (16 hours light at 24°C and 8 hours
814 darkness at 22°C). Seven days after transfer to potting soil, the seedlings were
815 inoculated with mycelium of a 14-day-old *R. necatrix* culture in PDB. To this end,
816 the mycelium was pelleted, washed, and resuspended in 250 mL water. This
817 mycelial suspension was subsequently used for root-dip inoculation of the cotton
818 seedlings for 10 min, after which they were re-planted and 10 mL of mycelium
819 suspension was poured onto the pot in close proximity to the stem. At 14 days
820 post inoculation (dpi) disease symptoms were recorded. The experiment was
821 repeated three times.
822
823 **Data availability**
824 Genomes and genome annotation data have been submitted to NCBI under
825 BioProject PRJNA727191.

826

827 **Supporting information**

828 **Supplemental Table 1. Annotation of predicted effector proteins of *R.***
829 ***necatrix* strain R18.**

830 **Supplemental Table 2. Annotated secondary metabolite clusters of *R.***
831 ***necatrix* strain R18.**

832 **Supplemental Table 3. Bacterial strains used in this study.**

833 **Supplemental Table 4. Primers used in this study.**

834 **Supplemental Table 5:** FUN_004580 homologs.

835 **Supplemental Table 6:** FUN_011519 homologs.

836

837 **Acknowledgements**

838 EACC and DET acknowledge receipt of PhD fellowships from CONACyT, Mexico.
839 ALM is holder of a postdoctoral research fellow funded by the 'Fundación Ramón
840 Areces'. BPHJT acknowledges funding by the Alexander von Humboldt Foundation
841 in the framework of an Alexander von Humboldt Professorship endowed by the
842 German Federal Ministry of Education and Research, and is furthermore
843 supported by the Deutsche Forschungsgemeinschaft (DFG, German Research
844 Foundation) under Germany´s Excellence Strategy – EXC 2048/1 – Project ID:
845 390686111. The authors declare no conflict of interest exists.

846

847 **Author contributions**

848 Conceptualization: Edgar Chavarro-Carrero, Nick Snelders, Michael Seidl, Bart
849 Thomma.

850 Formal analysis: Edgar Chavarro-Carrero, Nick Snelders, David Torres, Anton
851 Kraege.

Investigation: Edgar Chavarro-Carrero, Nick Snelders, David Torres, Anton Kraege.

Resources: Ana López-Moral, Gabriella Petti, Wilko Punt, Jan Wieneke, Rómulo García-Velasco, Carlos López-Herrera.

Supervision: Nick Snelders, Michael Seidl, Bart Thomma.

Writing – Original Draft Preparation: Edgar Chavarro-Carrero, Nick Snelders, David Torres, Anton Kraege.

Writing – Review & Editing: Michael Seidl, Bart Thomma.

860 **REFERENCES**

861 Almagro, J. J. A., Tsirigos, K. D., Sønderby, C. K., Petersen, T. N., Winther, O.,
862 Brunak, S., von Heijne, G., and Nielsen, H. (2019). SignalP 5.0 improves
863 signal peptide predictions using deep neural networks. Nature
864 Biotechnology, 37: 420-423.

865 Badri, D. V., and Vivanco, J. M. (2009). Regulation and function of root exudates.
866 Plant Cell and Environment, 32: 666-681.

867 Bailly-Bechet, M., Haudry, A., and Lerat, E. (2014). "One code to find them all":
868 a perl tool to conveniently parse RepeatMasker output files. Mobile DNA, 5:
869 1-15.

870 Bray, N. L., Pimentel, H., Melsted, P., and Pachter, L. (2016). Near-optimal
871 probabilistic RNA-seq quantification. Nature Biotechnology, 34: 525-527.

872 Beilsmith, K., Thoen, M. P. M., Brachi, B., Gloss, A. D., Khan, M. H., and
873 Bergelson, J. (2019). Genome-wide association studies on the
874 phyllosphere microbiome: Embracing complexity in host–microbe
875 interactions. The Plant Journal, 97: 164-181.

876 Berendsen, R. L., Pieterse, C. M. J., and Bakker, P. A. H. M. (2012). The
877 rhizosphere microbiome and plant health. Trends in Plant Science, 17:
878 478-486.

879 Bertels, F., Silander, O. K., Pachkov, M., Rainey, P. B., and van Nimwegen, E.
880 (2014). Automated reconstruction of whole-genome phylogenies from
881 short-sequence reads. Molecular Biology and Evolution, 31: 1077-1088.

882 Blin, K., Shaw, S., Steinke, K., Villebro, R., Ziemert, N., Lee, S. Y., Medema, M.
883 H., and Weber, T. (2019). AntiSMASH 5.0: updates to the secondary
884 metabolite genome mining pipeline. Nucleic Acids Research, 47: 81–87.

885 Bormann, C., Baier, D., Hörr, I., Raps, C., Berger, J., Jung, G., and Schwarz, H.
886 (1999). Characterization of a novel, antifungal, chitin-binding protein from
887 *Streptomyces tendae* Tu□901 that interferes with growth polarity. Journal
888 of Bacteriology, 181: 7421-7429.
889 Bressan, M., Roncato, M., Bellvert, F., Comte, G., Haichar, F., Achouak, W., and
890 Berge, O. (2009). Exogenous glucosinolate produced by *Arabidopsis*
891 *thaliana* has an impact on microbes in the rhizosphere and plant roots.
892 Multidisciplinary Journal of Microbial Ecology, 3: 1243–1257.
893 Broekaert, W. F., Marien, W., Terras, F. R. G., De Bolle, M. F. C., Proost, P., Van
894 Damme, J., Dillen, L., Claeys, M., Rees, A. B., Vanderleyden, J., and
895 Cammue, B. P. A. (1992). Antimicrobial peptides from *Amaranthus*
896 *caudatus* seeds with sequence homology to the cysteine/glycine-rich
897 domain of chitin-binding proteins. Biochemistry, 31: 4308-4314.
898 Burton, J. N., Adey, A., Patwardhan, R. P., Qiu, R., Kitzman, J. O., and Shendure,
899 J. (2013). Chromosome-scale scaffolding of *de novo* genome assemblies
900 based on chromatin interactions. Nature Biotechnology, 31: 1119–1125.
901 Campos-Olivas, R., Hörr, I., Bormann, C., Jung, G., and Gronenborn, A. M.
902 (2001). Solution structure, backbone dynamics and chitin binding of the
903 anti-fungal protein from Streptomyces tendae TÜ901. Journal of Molecular
904 Biology, 308: 765-782.
905 Carresi, L., Pantera, B., Zoppi, C., Cappugi, G., Oliveira, A. L., Pertinhez, T. A.,
906 Spisni, A., Scala, A., and Pazzagli, L. (2006). Cerato-platanin, a phytotoxic
907 protein from *Ceratocystis fimbriata*: expression in *Pichia pastoris*,
908 purification and characterization. Protein Expression and Purification, 49:
909 159-167.

910 Cazorla, F. M., Duckett, S. B., Bergström, E. T., Noreen, S., Odijk, R.,
911 Lugtenberg, B. J. J., Thomas-Oates, J. E., and Bloemberg, G. V. (2006).
912 Biocontrol of avocado dematophora root rot by antagonistic *Pseudomonas*
913 *fluorescens* PCL1606 correlates with the production of 2-hexyl 5-propyl
914 resorcinol. Molecular Plant-Microbe Interactions, 19: 418–428.
915 Chai, Y. N., and Schachtman, D. P. (2022). Root exudates impact plant
916 performance under abiotic stress. Trends in Plant Science, 27: 80-91.
917 Chavarro-Carrero, E. A., Vermeulen, J. P., E. Torres, D., Usami, T., Schouten, H.
918 J., Bai, Y., Seidl, M. F., and Thomma, B. P. H. J. (2021). Comparative
919 genomics reveals the in planta-secreted *Verticillium dahliae* Av2 effector
920 protein recognized in tomato plants that carry the *V2* resistance locus.
921 Environmental Microbiology, 23: 1941–1958.
922 Cook, D., Donzelli, B. G. G., Creamer, R., Baucom, D. L., Gardner, D. R., Pan, J.,
923 Moore, N., Krasnoff, S. B., Jaromczyk, J. W., and Schardl, C. L. (2017).
924 Swainsonine biosynthesis genes in diverse symbiotic and pathogenic fungi.
925 Genes, Genomes, Genetics, 7: 1791-1797.
926 Cordovez, V., Rotoni, C., Dini-Andreote, F., Oyserman, B., Carrión, V. J., and
927 Raaijmakers, J. M. (2021). Successive plant growth amplifies genotype-
928 specific assembly of the tomato rhizosphere microbiome. Science of the
929 Total Environment, 772: 144825.
930 Danecek, P., Bonfield, J. K., Liddle, J., Marshall, J., Ohan, V., Pollard, M. O.,
931 Whitwham, A., Keane, T., McCarthy, S. A., Davies, R. M., and Li, H.
932 (2021). Twelve years of SAMtools and BCFtools. Gigascience, 10: 1-4.
933 Davey, J. W., Davis, S. J., Mottram, J. C., and Ashton, P. D. (2020). Tapestry:
934 validate and edit small eukaryotic genome assemblies with long reads.
935 BioRxiv, 2019–2020.

936 de Guillen, K., Ortiz-Vallejo, D., Gracy, J., Fournier, E., Kroj, T., and Padilla, A.
937 (2015). Structure analysis uncovers a highly diverse but structurally
938 conserved effector family in phytopathogenic fungi. PLoS Pathogens, 11:
939 1-27.
940 de Jonge, R., and Thomma, B. P. H. J. (2009). Fungal LysM effectors:
941 extinguishers of host immunity? Trends in Microbiology, 17: 151–157.
942 de Jonge, R., van Esse, H. P., Kombrink, A., Shinya, T., Desaki, Y., Bours, R.,
943 van der Krol, S., Shibuya, N., Joosten, M. H. A. J., and Thomma, B. P. H.
944 J. (2010). Conserved fungal LysM effector Ecp6 prevents chitin-triggered
945 immunity in plants. Science, 329: 953-955.
946 Djamei, A., Schipper, K., Rabe, F., Ghosh, A., Vincon, V., Kahnt, J., Osorio, S.,
947 Toghe, T., Fernie, A. R., Feussner, K., Meinicke, P., Stierhof; Y., Schwarz,
948 H., Macek, B., Mann, M., and Kahmann, R. (2011). Metabolic priming by a
949 secreted fungal effector. Nature, 478: 395-398.
950 Dong, S., Raffaele, S., and Kamoun, S. (2015). The two-speed genomes of
951 filamentous pathogens: waltz with plants. Current Opinion in Genetics and
952 Development, 35: 57-65.
953 Dudchenko, O., Batra, S. S., Omer, A. D., Nyquist, S. K., Hoeger, M., Durand, N.
954 C., Shamin, M. S., Machol, I., Lander, E. S., Aiden, A. P., and Aiden, E. L.
955 (2017). *De novo* assembly of the *Aedes aegypti* genome using Hi-C yields
956 chromosome-length scaffolds. Science, 356: 92–95.
957 Dudchenko, O., Shamim, M. S., Batra, S. S., Durand, N. C., Musial, N. T.,
958 Mostofa, R., Pham, M., St Hilaire, B. G., Yao, W., Stamenova, E., Hoeger,
959 M., Nyquist, S., Korchina, V., Pletch, K., Flanagan, J. P., Tomaszewicz, A.,
960 McAloose, D., Perez-Estrada, C., Novak, B. J., Omer, R. D., and Aiden, E.
961 L. (2018). The juicebox assembly tools module facilitates *de novo*

962 assembly of mammalian genomes with chromosome-length scaffolds for
963 under $1000. BioRxiv, 254797.
964 Duplessis, S., Cuomo, C. A., Lin, Y., Aerts, A., Tisserant, E., Veneault-Fourrey,
965 C., Joly, D., Hacquard, S., Amselem, J., Cantarel, B. L. Chiu, R., Coutinho,
966 P. M., Feau, N., Field, M., Frey, P., Gelhaye, E., Goldberg, J., Grabherr, M.
967 G., Kodira, C. D., Kohler, A., Kües, U., Lindquist, E. A., Lucas, S. M., Mago,
968 R., Mauceli, E., Morin, E., Murat, C., Pangilinan, J. L., Park, R., Pearson,
969 M., Quesneville, H., Rouhier, N., Sakthikumar, S., Salamov, A., Schmutz,
970 J., Selles, B., Shapiro, H., Tanguay, P., Tuskan, G. A., Henrissat, B., van
971 de Peer, Y., Rouzé, P., Ellis, J. G., Dodds, P. N., Schein, J. E., Zhong, S.,
972 Hamelin, R. C., Grigoriev, I. V., Szabo, L. J., and Martin, F. (2011).
973 Obligate biotrophy features unraveled by the genomic analysis of rust
974 fungi. Proceedings of the National Academy of Sciences, 108: 9166-9171.
975 Durand, N. C., Shamim, M. S., Machol, I., Rao, S. S. P., Huntley, M. H., Lander,
976 E. S., and Aiden, E. L. (2016). Juicer provides a one-click system for
977 analyzing loop-resolution Hi-C experiments. Cell Systems, 3: 95–98.
978 Eguchi, N., Kondo, K. I., and Yamagishi, N. (2009). Bait twig method for soil
979 detection of *Rosellinia necatrix*, causal agent of white root rot of Japanese
980 pear and apple, at an early stage of tree infection. Journal of General Plant
981 Pathology, 75: 325–330.
982 Faino, L., Seidl, M. F., Shi-Kunne, X., Pauper, M., van den Berg, G. C.,
983 Wittenberg, A. H., and Thomma, B. P. H. J. (2016). Transposons passively
984 and actively contribute to evolution of the two-speed genome of a fungal
985 pathogen. Genome Research, 26: 1091–1100.
986 Fouché, S., Badet, T., Oggenfuss, U., Plissonneau, C., Francisco, C. S., and Croll,
987 D. (2020). Stress-driven transposable element de-repression dynamics

988 and virulence evolution in a fungal pathogen. Molecular Biology and
989 Evolution, 37: 221-239.
990 Frantzeskakis, L., Di Pietro, A., Rep, M., Schirawski, J., Wu, C., and Panstruga,
991 R. (2020). Rapid evolution in plant–microbe interactions – a molecular
992 genomics perspective. Plant Phytologist, 225: 1134-1142.
993 Frantzeskakis, L., Kracher, B., Kusch, S., Yoshikawa-Maekawa, M., Bauer, S.,
994 Pedersen, C., Spanu, P. D., Maekawa, T., Schulze-Lefert, P., and
995 Panstruga, R. (2018). Signatures of host specialization and a recent
996 transposable element burst in the dynamic one-speed genome of the
997 fungal barley powdery mildew pathogen. BMC Genomics, 19: 381.
998 Freitas, D. A., Leclerc, S., Miyoshi, A., Oliveira, S. C., Sommer, P. S. M.,
999 Rodrigues, L., Correa-Junior, A., Gautier, M., Langella, P., Azevedo, V. A.,
1000 and Le Loir, Y. (2005). Secretion of *Streptomyces tendae* antifungal
1001 protein 1 by *Lactococcus lactis*. Brazilian Journal of Medical and Biological
1002 Research, 38: 1585-1592.
1003 Gan, P., Ikeda, K., Irieda, H., Narusaka, M., O'Connell, R. J., Narusaka, Y.,
1004 Takano, Y., Kubo, Y., and Shirasu, K. (2013). Comparative genomic and
1005 transcriptomic analyses reveal the hemibiotrophic stage shift of
1006 *Colletotrichum* fungi. New Phytologist, 197: 1236-1249.
1007 García-velasco, R., González-díaz, J. G., Domínguez-arizmendi, G., Ayala-
1008 escobar, V., and Aguilar-medel, S. (2012). *Rosellinia necatrix* in *Rosa* sp.,
1009 and an evaluation of its sensitivity to fungicides. Revista Chapingo, Serie
1010 Horticultura, 18: 39–54.
1011 Gel, B., Díez-Villanueva, A., Serra, E., Buschbeck, M., Peinado, M. A., and
1012 Malinverni, R. (2016). regioneR: an R/Bioconductor package for the

1013 association analysis of genomic regions based on permutation tests.
1014 Bioinformatics, 32: 289–291.
1015 Guillaumin, J., Mercier, S., and Dubos, B. (1982). Les pourridiés à Armillariella et
1016 Rosellinia en France sur vigne, arbres fruitiers et cultures florales I.
1017 Etiologie et symptomatologie. Agronomie, 2: 71–80.
1018 Ingham, A. B., and Moore, R. J. (2007). Recombinant production of antimicrobial
1019 peptides in heterologous microbial systems. Biotechnology and Applied
1020 Biochemistry, 47: 1-9.
1021 Ismail, I. A., and Able, A. (2016). Secretome analysis of virulent *Pyrenophora*
1022 *teres* f. *teres* isolates. Proteomics, 16: 2625-2636.
1023 Jeffares, D. C., Jolly, C., Hoti, M., Speed, D., Shaw, L., Rallis, C., Balloux, F.,
1024 Dessimoz, C., Bähler, J., and Sedlazeck, F. J. (2017). Transient structural
1025 variations have strong effects on quantitative traits and reproductive
1026 isolation in fission yeast. Nature Communications, 8: 1-11.
1027 Jumper, J., Evans, R., Pritzel, A., Green, T., Figurnov, M., Ronneberger, O.,
1028 Tunyasuvunakool, K., Bates, R., Žídek, A., Potapenko, A., Bridgland, A.,
1029 Meyer, C., Kohl, S. A. A., Ballard, A. J., Cowie, A., Romera-Paredes, B.,
1030 Nikolov, S., Jain, R., Adler, J., Back, T., Petersen, S., Reiman, D., Clancy,
1031 E., Zielinski, M., Steinegger, M., Pacholska, M., Berghammer, T.,
1032 Bodenstein, S., Silver, D., Vinyals, O., Senior, A. W., Kavukcuoglu, K.,
1033 Kohli, P., and Hassabis, D. (2021). Highly accurate protein structure
1034 prediction with AlphaFold. Nature, 596: 583–589.
1035 Katoh, K., and Standley, D. M. (2013). MAFFT multiple sequence alignment
1036 software version 7: Improvements in performance and usability. Molecular
1037 Biology and Evolution, 30: 772–780.

1038 Kawaide, H. (2006). Biochemical and molecular analyses of gibberellin
1039 biosynthesis in fungi. Bioscience, Biotechnology, and Biochemistry, 70:
1040 583-590.
1041 Kelley, L. A., Mezulis, S., Yates, C. M., Wass, M. N., and Sternberg, M. J. E.
1042 (2015). The Phyre2 web portal for protein modeling, prediction and
1043 analysis. Nature Protocols, 10: 845-858.
1044 Kombrink, A., and Thomma, B. P. H. J. (2013). LysM effectors: secreted proteins
1045 supporting fungal life. PLoS Pathogens, 9: 1–4.
1046 Koren, S., Walenz, B. P., Berlin, K., Miller, J. R., Bergman, N. H., and Phillippy,
1047 A. M. (2017). Canu: scalable and accurate long-read assembly via
1048 adaptive k-mer weighting and repeat separation. Genome Research, 27:
1049 722–736.
1050 Langmead, B., and Salzberg, S. L. (2012). Fast gapped-read alignment with
1051 Bowtie 2. Nature Methods, 9: 357–359.
1052 Lenarčič, T., Albert, I., Böhm, H., Hodnik, V., Pirc, K., Zavec, A. B., Podobnik, M.,
1053 Pahovnik, D., Žagar, E., Pruitt, R., Greimel, P., Yamaji-Hasegawa, A.,
1054 Kobayashi, T., Zienkiewicz, A., Gömann, J., Mortimer, J. C., Fang, L.,
1055 Mamode-Cassim, A., Deleu, M., Lins, L., Oecking, C., Feussner, I.
1056 Mongrand, S., Anderluh, G., and Nürnberger, T. (2017). Eudicot plant-
1057 specific sphingolipids determine host selectivity of microbial NLP
1058 cytolysins. Science, 358: 1431-1434.
1059 Lo Presti, L., Lanver, D., Schweizer, G., Tanaka, S., Liang, L., Tollot, M., Zuccaro,
1060 A., Reissmann, S., and Kahmann, R. (2015). Fungal effectors and plant
1061 susceptibility. The Annual Review of Plant Biology, 66: 513-545.
1062 Lu, Y., Xue, Q., Eisele, M. R., Sulistijo, E. S., Brower, K., Han, L., Amir, E. D.,
1063 Pe'er, D., Miller-Jensen, K., and Fan, R. (2015). Highly multiplexed

1064 profiling of single-cell effector functions reveals deep functional
1065 heterogeneity in response to pathogenic ligands. Proceedings of the
1066 National Academy of Sciences, 112: E607-E615.
1067 Luciano-Rosario, D., Eagan, J. L., Aryal, N., Dominguez, E. G., Hull, C. M., and
1068 Keller, N. P. (2022). The hydrophobin gene family confers a fitness trade-
1069 off between spore dispersal and host colonization in *Penicillium expansum*.
1070 mBio, e02754-22.
1071 Malinovsky, F. G., Fangel, J. U., and Willats, W. G. T. (2014). The role of the cell
1072 wall in plant immunity. Frontiers in Plant Science, 5: 1-12.
1073 Martins, J. C., Maes, D., Loris, R., Pepermans, H. A. M., Wyns, L., Willen, R., and
1074 Verheyden, P. (1996). ^{1}H NMR study of the solution structure of Ac-AMP2,
1075 a sugar binding antimicrobial protein isolated from *Amaranthus caudatus*.
1076 Journal of Molecular Biology, 258: 322-333.
1077 Oggenfuss, U., Badet, T., Wicker, T., Hartmann, F. E., Singh, N. K., Abraham, L.,
1078 Karisto, P., Vonlanthen, T., Mundt, C., McDonald, B. A., and Croll, D.
1079 (2021). A population-level invasion by transposable elements triggers
1080 genome expansion in a fungal pathogen. eLife, 10: e69249.
1081 Ou, S., Su, W., Liao, Y., Chougule, K., Agda, J. R. A., Hellinga, A. J., Blanco-
1082 Lugo, C. S., Elliot, T. A., Waren, D., Peterson, T., Jiang, N., Hirsch, C. N.,
1083 and Hufford, M. B. (2019). Benchmarking transposable element annotation
1084 methods for creation of a streamlined, comprehensive pipeline. Genome
1085 Biology, 20: 275.
1086 Palmer, J., and Stajich, J. E. (2017). Funannotate: Eukaryotic genome
1087 annotation pipeline. Retrieved from
1088 https://funannotate.readthedocs.io/en/latest/

1089 Pérez-Jaramillo, J. E., Mendes, R., and Raaijmakers, J. M. (2016). Impact of
1090 plant domestication on rhizosphere microbiome assembly and functions.
1091 Plant Molecular Biology, 90: 635-644.
1092 Pérez-Jiménez, R. M., Jiménez-Díaz, R. M., and López-Herrera, C. J. (2002).
1093 Somatic incompatibility of *Rosellinia necatrix* on avocado plants in
1094 southern Spain. Mycological Research, 106: 239–244.
1095 Pliego, C., Kanematsu, S., Ruano-Rosa, D., de Vicente, A., López-Herrera, C.,
1096 Cazorla, F. M., and Ramos, C. (2009). GFP sheds light on the infection
1097 process of avocado roots by *Rosellinia necatrix*. Fungal Genetics and
1098 Biology, 46: 137–145.
1099 Quinlan, A. R., and Hall, I. M. (2010). BEDTools: a flexible suite of utilities for
1100 comparing genomic features. Bioinformatics, 26: 841-842.
1101 Rademacher, W., and Graebe, J. E. (1979). Gibberellin A4 produced by
1102 *Sphaceloma manihoticola*, the cause of the super elongation disease of
1103 cassava (*Manihot esculenta*). Biochemical and Biophysical Research
1104 Communications, 91: 35-40.
1105 Rafaelle, S., Farrer, R. A., Cano, L. M., Studholme, D. J., Maclean, D., Thines, M.,
1106 Jiang, R. H. Y., Zody, M. C., Kunjeti, S. G., Donofrio, N. M., Meyers, B. C.,
1107 Nusbaum, C., and Kamoun, S. (2010). Genome evolution following host
1108 jumps in the irish potato famine pathogen lineage. Science, 330: 1540-
1109 1543.
1110 Raffaele, S., and Kamoun, S. (2012). Genome evolution in filamentous plant
1111 pathogens: why bigger can be better. Nature Reviews Microbiology, 10:
1112 417-430.
1113 Rocafort, M., Bowen, J. K., Hassing, B., Cox, M. P., McGreal, B., de la Rosa, S.,
1114 Plummer, K. M., Bradshaw, R. E., and Mesarich, C. H. (2022). The

1115 *Venturia inaequalis* effector repertoire is dominated by expanded families
1116 with predicted structural similarity, but unrelated sequence, to avirulence
1117 proteins from other plant-pathogenic fungi. BMC Biology, 20: 1-24.
1118 Rovenich, H., Boshoven, J. C., and Thomma, B. P. H. J. (2014). Filamentous
1119 pathogen effector functions: of pathogens, hosts and microbiomes.
1120 Current Opinion in Plant Biology, 20: 96-103.
1121 Santhanam, P., Van Esse, H.P., Albert, I., Faino, L., Nürnberger, T., and
1122 Thomma, B.P.H.J. (2013). Evidence for functional diversification within a
1123 fungal Nep1-like protein family. Molecular Plant Microbe Interactions, 26:
1124 278–286.
1125 Sawai, K., Okuno, T., Fujioka, H., and Furuya, M. (1983). The relation between
1126 the phytotoxicity of Cythochalasin E and its molecular structure. Annals of
1127 the Phytopathological Society of Japan, 49: 262-265.
1128 Schwessinger, B., Sperschneider, J., Cuddy, W. S., Garnica, D. P., Miller, M. E.,
1129 Taylor, J. M., Dodds, P. N., Figueroa, M., Park, R. F., and Rathjen, J. P.
1130 (2018). A near-complete haplotype-phased genome of the dikaryotic
1131 wheat stripe rust fungus *Puccinia striiformis* f. sp. *Tritici* reveals high
1132 interhaplotype diversity. mBio, 9: e02275-17.
1133 Seidl, M. F., and Thomma, B. P. H. J. (2014). Sex or no sex: evolutionary
1134 adaptation occurs regardless. Bioessays, 36: 335-345.
1135 Seidl, M. F., and Thomma, B. P. H. J. (2017). Transposable elements direct the
1136 coevolution between plants and microbes. Trends in Genetics, 33: 842–
1137 851.
1138 Seidl, M. F., and van den Ackerveken, G. (2019). Activity and phylogenetics of
1139 the broadly occurring family of microbial nep1-like proteins. Annual Review
1140 of Phytopathology, 57: 367–386.

1141 Seidl, M. F., Kramer, H. M., Cook, D. E., Fiorin, G. L., van den Berg, G. C. M.,
1142 Faino, L., and Thomma, B. P. H. J. (2020). Repetitive elements contribute
1143 to the diversity and evolution of centromeres in the fungal genus
1144 *verticillium*. MBio, 11: 1–22.
1145 Shi-Kunne, X., Faino, L., van den Berg G. C. M., Thomma B. P. H. J., and Seidl,
1146 M. F. (2018). Evolution within the fungal genus *Verticillium* is characterized
1147 by chromosomal rearrangement and gene loss. Environmental
1148 Microbiology, 20: 1362-1373.
1149 Shimizu, T., Kanematsu, S., and Yaegashi, H. (2018). Draft genome sequence
1150 and transcriptional analysis of *Rosellinia necatrix* infected with a virulent
1151 mycovirus. Phytopathology, 108: 1206–1211.
1152 Shimizu, T., Tsutae, I., and Kanematsu, S. (2014). Functional analysis of a
1153 melanin biosynthetic gene using RNAi-mediated gene silencing in *Rosellinia*
1154 *necatrix*. Fungal Biology, 118: 413-421.
1155 Simão, F. A., Waterhouse, R. M., Ioannidis, P., Kriventseva, E. V., and Zdobnov,
1156 E. M. (2015). BUSCO: Assessing genome assembly and annotation
1157 completeness with single-copy orthologs. Bioinformatics, 31: 3210–3212.
1158 Sivanesan, A., and Holliday, P. (1972). *Rosellinia necatrix*. In Description of
1159 Pathogenic Fungi and Bacteria, (p. 352).
1160 Smercina, D. N., Bailey, V. L., and Hofmockel, K. S. (2021). Micro on a
1161 macroscale: relating microbial-scale soil processes to global ecosystem
1162 function. FEMS Microbiology Ecology, 97: 1-11.
1163 Snelders, N. C., Boshoven, J. C., Song, Y., Schmitz, N., Fiorin, G. L., Rovenich,
1164 H., van den Berg, G. C. M., Torres, D. E., Petti, G. C., Prockl, Z., Faino, L.,
1165 Seidl, M. F., and Thomma, B. P. H. J. (2023). A highly polymorphic effector

1166 protein promotes fungal virulence through suppression of plant-associated
1167 Actinobacteria. New Phytologist, doi:10.1111/nph.18576
1168 Snelders, N. C., Kettles, G. J., Rudd, J. J., and Thomma, B. P. H. J. (2018). Plant
1169 pathogen effector proteins as manipulators of host microbiomes? Molecular
1170 Plant Pathology, 19: 257-259.
1171 Snelders, N. C., Petti, G. C., van den Berg, G. C. M., Seidl, M. F., and Thomma,
1172 B. P. H. J. (2021). An ancient antimicrobial protein co-opted by a fungal
1173 plant pathogen for *in planta* mycobiome manipulation. Proceedings of the
1174 National Academy of Sciences, 118: e2110968118.
1175 Snelders, N. C., Rovenich, H., and Thomma, B. P. H. J. (2022). Microbiota
1176 manipulation through the secretion of effector proteins is fundamental to
1177 the wealth of lifestyles in the fungal kingdom. FEMS Microbiology Reviews,
1178 46: 1-16.
1179 Snelders, N. C., Rovenich, H., Petti, G. C., Rocafort, M., van den Berg, G. C. M.,
1180 Vorholt, J. A., Mesters, J. R., Seidl, M., Nijland, R., and Thomma, B. P. H.
1181 J. (2020). Microbiome manipulation by a soil-borne fungal plant pathogen
1182 using effector proteins. Nature Plants, 6: 1365-1374.
1183 Spanu, P. D. (2017). Cereal immunity against powdery mildews targets RNase-
1184 Like Proteins associated with Haustoria (RALPH) effectors evolved from a
1185 common ancestral gene. New Phytologist, 213: 1301-1314.
1186 Sperschneider, J., Dodds, P. N., Gardiner, D. M., Singh, K. B., and Taylor, J. M.
1187 (2018). Improved prediction of fungal effector proteins from secretomes
1188 with EffectorP 2.0. Molecular Plant Pathology, 19: 2094-2110.
1189 Stamatakis, A. (2014). RAxML version 8: A tool for phylogenetic analysis and
1190 post-analysis of large phylogenies. Bioinformatics, 30: 1312–1313.

1191 Stancu, M. C., Van Roosmalen, M. J., Renkens, I., Nieboer, M. M., Middelkamp,
1192 S., de Ligt, J., Pregno, G., Giachino, D., Mandrile, G., Espejo, J. V.,
1193 Korzelius, J., de Bruijn, E., Cuppen, E., Talkowski, M. E., Marschall, T., de
1194 Ridder, J., and Kloosterman, W. P. (2017). Mapping and phasing of
1195 structural variation in patient genomes using nanopore sequencing. Nature
1196 Communications, 8: 1–13.
1197 Stergiopoulos, I., Collemare, J., Mehrabi, R., and de Wit, P. J. G. M. (2013).
1198 Phytotoxic secondary metabolites and peptides produced by plant
1199 pathogenic *Dothideomycete* fungi. FEMS Microbiology Review, 37: 67-93.
1200 Sztejnberg, A., and Madar, Z. (1980). Host range of *Dematophora necatrix*, the
1201 cause of white root rot disease in fruit trees. Plant Disease, 64: 662–664.
1202 Takai, S. (1974). Pathogenicity and cerato-ulmin production in *Ceratocystis ulmi*.
1203 Nature, 252: 124-126.
1204 Talbot, N. J., Kershaw, M. J., Wakley, G. E., de Vries, O. M. H., Wessels, J. G. H.,
1205 and Hamer, J. E. (1996). *MPG1* encodes a fungal hydrophobin involved in
1206 surface interaction during infection-related development of *Magnaporthe*
1207 *grisea*. The Plant Cell, 8: 985-999.
1208 Thomas, D. D. (1978). Cytochalasin effects in plants and eukaryotic microbial
1209 systems. Frontiers in Biology, 46: 257-275.
1210 Thomma, B. P. H. J., Seidl, M. F., Shi-Kunne, X., Cook, D. E., Bolton, M. D., van
1211 Kan, J. A. L., and Faino, L. (2016). Mind the gap; seven reasons to close
1212 fragmented genome assemblies. Fungal Genetics and Biology, 90: 24–30.
1213 Tian, H., Fiorin, G. L., Kombrink, A., Mesters, J. R., and Thomma, B. P. H. J.
1214 (2022). Fungal dual-domain LysM effectors undergo chitin-induced
1215 intermolecular, and not intramolecular, dimerization. Plant Physiology,
1216 190: 2033-2044.

1217 Tian, H., MacKenzie, C. I., Rodriguez-Moreno, L., van den Berg, G. C. M., Chen,
1218 H., Rudd, J. J., Mesters, J. R., and Thomma, B. P. H. J. (2021). Three LysM
1219 effectors of Zymoseptoria tritici collectively disarm chitin-triggered plant
1220 immunity. Molecular Plant Pathology, 22: 683-693.
1221 Törönen, P., and Holm, L. (2022). PANNZER-A practical tool for protein function
1222 prediction. Protein Science, 31: 118-128.
1223 Torres, D. E., Oggenfuss, U., Croll, D., and Seidl, M. (2020). Genome evolution
1224 in fungal plant pathogens: looking beyond the two-speed genome model.
1225 Fungal Biology Reviews, 34: 136-143.
1226 Underwood, W. (2012). The plant cell wall: a dynamic barrier against pathogen
1227 invasion. Frontiers in Plant Science, 3: 1-6.
1228 Varoquaux, N., Liachko, I., Ay, F., Burton, J. N., Shendure, J., Dunham, M. J.,
1229 Vert, J. P., and Noble, W. S. (2015). Accurate identification of centromere
1230 locations in yeast genomes using Hi-C. Nucleic Acids Research, 43: 5331–
1231 5339.
1232 Virtanen, P., Gommers, R., Oliphant, T. E., Haberland, M., Reddy, T.,
1233 Cournapeau, D., Burovski, E., Peterson, P., Weckesser, W., Bright, J., van
1234 der Walt, S. J., Brett, M., Wilson, J., Millman, K. J., Mayorov, N., Nelson, A.
1235 R. J., Jones, E., Kern, R., Larson, E., Carey, C. J., Polat, İ., Feng, Y.,
1236 Moore, E. W., VanderPlas, J., Laxalde, D., Perktold, J., Cimrman, R.,
1237 Henriksen, I., Quintero, E. A., Harris, C. R., Archibald, A. M., Ribeiro, A.,
1238 Pedregosa, F., van Mulbregt, P., and SciPy 1.0 Contributors. (2020). SciPy
1239 1.0: fundamental algorithms for scientific computing in Python. Nature
1240 Methods, 17: 261–272.

1241 Walton, J. D. (1990). Peptide phytotoxins from plant pathogenic fungi. In
1242 Biochemistry of peptide antibiotics. Kleinkauf, H., and von Dohren, H.
1243 (eds). Berlin, 179-203 pp.
1244 Wang, E., Schornack, S., Marsh, J. F., Gobbato, E., Schwessinger, B., Eastmond,
1245 P., Schultze, M., Kamoun, S., and Oldroyd, G. E. D. (2012). A common
1246 signaling process that promotes Mycorrhizal and Oomycete colonization of
1247 plants. Current Biology, 22: 2242-2246.
1248 Wang, J. R., Holt, J., McMillan, L., and Jones, C. D. (2018). FMLRC: Hybrid long
1249 read error correction using an FM-index. BMC Bioinformatics, 19: 1–11.
1250 Wawra, S., Fesel, P., Widmer, H., Neumann, U., Lahrmann, U., Becker, S.,
1251 Hehemann, J., Langen, G., and Zuccaro, A. (2019). FGB1 and WSC3 are *in*
1252 *planta*-induced *β*-glucan-binding fungal lectins with different functions.
1253 New Phytologist, 222: 1493-1506.
1254 Weiberg, A., Wang, M., Bellinger, M., and Jin, H. (2014). Small RNAs: a new
1255 paradigm in plant-microbe interactions. The Annual Review of
1256 Phytopathology, 52: 495-516.
1257 Weinert, N. Piceno, Y., Ding, G., Meincke, R., Heuer, H., Berg, G., Schloter, M.,
1258 Andersen, G., and Smalla, K. (2011). PhyloChip hybridization uncovered
1259 an enormous bacterial diversity in the rhizosphere of different potato
1260 cultivars: many common and few cultivar-dependent taxa. FEMS
1261 Microbiology Ecology, 75: 497-506.
1262 Wick, R. (2018). Porechop. Retrieved from https://github.com/rrwick/Porechop
1263 Wilson, R. A., and McDowell, J. M. (2022). Recent advances in understanding of
1264 fungal and oomycete effectors. Current Opinion in Plant Biology, 68:
1265 102228.

Wingfield, B. D., Berger, D. K., Coetzee, M. P. A., Duong, T. A., Martin, A., Pham, N. Q., van den Berg, N., Wilken, P. M., Arun Chinnappa, K. S., Barnes, I., Buthelezi, S., Dahanayaka, B. A., Durán, A., Engelbrecht, J., Feurtey, A., Fourie, A., Fourie, G., Hartley, J., Kabwe, E. N. K., Maphosa, M., Mensah, D. L. N., Nsibo, D. L., Potgieter, L., Poudel, B., Stukenbrock, E. H., Thomas, C., Vaghefi, N., Welgemoed, T., and Wingfield, M. J. (2022). IMA genome-F17: Draft genome sequences of an *Armillaria* species from Zimbabwe, *Ceratocystis colombiana*, *Elsinoë necatrix*, *Rosellinia necatrix*, two genomes of *Sclerotinia minor*, short-read genome assemblies and annotations of four *Pyrenophora teres* isolates from barley grass, and a long-read genome assembly of *Cercospora zeina.* IMA Fungus, 13: 1-22.

Xu, D., Xue, M., Shen, Z., Jia, X., Hou, X., Lai, D., and Zhou, L. (2021). Phytotoxic secondary metabolites from fungi. Toxins, 13: 1-65.

Zhalnina, K., Louie, K. B., Hao, Z., Mansoori, N., Nunes de Rocha, U., Shi, S., Cho, H., Karaoz, U., Loqué, D., Bowen. B. P., Firestone, M. K., Northen, T. R., and Brodie, E. L. (2018). Dynamic root exudate chemistry and microbial substrate preferences drive patterns in rhizosphere microbial community assembly. Nature Microbiology, 3: 470-480.

Zhao, Z., Ying, Y., Hung, Y., and Tang, Y. (2019). Genome mining reveals *Neurospora crassa* can produce the salicylaldehyde sordarial. Journal of Natural Products, 82: 1029-1033.

Zhang, Y., and Skolnick J. (2005). TM-align: a protein structure alignment algorithm based on the TM-score. Nucleid Acids Research, 33: 2302–2309.